

1 **Modelling winter organic aerosol at the European scale**
2 **with CAMx: evaluation and source apportionment with a**
3 **VBS parameterization based on novel wood burning smog**
4 **chamber experiments**

5 **Giancarlo Ciarelli¹, Sebnem Aksoyoglu¹, Imad El Haddad¹, Emily A. Bruns¹,**
6 **Monica Crippa², Laurent Poulain³, Mikko Äijälä⁴, Samara Carbone⁵, Evelyn**
7 **Freney⁶, Colin O'Dowd⁷, Urs Baltensperger¹ and André S. H. Prévôt¹**

8 [1]{Paul Scherrer Institute, Laboratory of Atmospheric Chemistry, 5232 Villigen PSI,
9 Switzerland}

10 [2]{European Commission, Joint Research Centre (JRC), Directorate for Energy, Transport
11 and Climate, Air and Climate Unit, Via E. Fermi 2749, I-21027 Ispra (VA), Italy}

12 [3]{Leibniz-Institute for Tropospheric Research (TROPOS), Permoserstr. 15, 04318 Leipzig,
13 Germany}

14 [4]{University of Helsinki, Department of Physics, Helsinki, Finland}

15 [5]{Institute of Physics, University of São Paulo, Rua do Matão Travessa R, 187, 05508-090
16 São Paulo, S.P., Brazil}

17 [6]{Laboratoire de Météorologie Physique (LaMP), CNRS/Université Blaise Pascal,
18 Clermont-Ferrand, France}

19 [7]{School of Physics and Centre for Climate & Air Pollution Studies, Ryan Institute,
20 National University of Ireland Galway, University Road, Galway, Ireland}

21
22
23 Correspondence to: S. Aksoyoglu (sebnem.aksoyoglu@psi.ch)

24 **Abstract**

25 We evaluated a modified VBS (Volatility Basis Set) scheme to treat biomass burning-like
26 organic aerosol (BBOA) implemented in CAMx (Comprehensive Air Quality Model with
27 extensions). The updated scheme was parameterized with novel wood combustion smog
28 chamber experiments using a hybrid VBS framework that accounts for a mixture of wood

29 burning organic aerosol precursors and their further functionalization and fragmentation in the
30 atmosphere. The new scheme was evaluated for one of the winter EMEP intensive campaigns
31 (February-March 2009) against aerosol mass spectrometer (AMS) measurements performed
32 at 11 sites in Europe. We found a considerable improvement for the modelled organic aerosol
33 (OA) mass compared to our previous model application with the mean fractional bias (MFB)
34 reduced from -61% to -29%.

35 We performed model-based source apportionment studies and compared results against
36 positive matrix factorization (PMF) analysis performed on OA AMS data. Both model and
37 observations suggest that OA was mainly of secondary origin at almost all sites. Modelled
38 secondary organic aerosol (SOA) contributions to total OA varied from 32 to 88% (with an
39 average contribution of 62%) and absolute concentrations were generally under-predicted.
40 Modelled primary hydrocarbon-like organic aerosol (HOA) and primary biomass burning-like
41 aerosol (BBPOA) fractions contributed to a lesser extent (HOA from 3 to 30%, and BBPOA
42 from 1 to 39%) with average contributions of 13 and 25%, respectively. Modelled BBPOA
43 fractions was found to represent 12 to 64% of the total residential heating related OA, with
44 increasing contributions at stations located in the northern part of the domain.

45 Source apportionment studies were performed to assess the contribution of residential and
46 non-residential combustion precursors to the total SOA. Non-residential combustion and road
47 transportation sector contributed about 30-40% to SOA formation (with increasing
48 contributions at urban and near industrialized sites) whereas residential combustion (mainly
49 related to wood burning) contributed to a larger extent, around 60-70%. Contributions to OA
50 from residential combustion precursors in different volatility ranges were also assessed: our
51 results indicate that residential combustion gas-phase precursors in the semivolatile range
52 (SVOC) contributed from 6 to 30%, with higher contributions predicted at stations located in
53 the southern part of the domain. On the other hand, the oxidation products of higher volatility
54 precursors (the sum of IVOCs and VOCs) contribute from 15 to 38% with no specific
55 gradient among the stations.

56 Although the new parameterization leads to a better agreement between model results and
57 observations, it still under-predicts the SOA fraction suggesting that uncertainties in the new
58 scheme and other sources and/or formation mechanisms remain to be elucidated. Moreover, a
59 more detailed characterization of the semivolatile components of the emissions is needed.

60 1 Introduction

61 Organic aerosol (OA) comprises the main fraction of fine particulate matter (PM_{10}) (Jimenez et
62 al., 2009). Even though the sources of its primary fraction (primary organic aerosol, POA) are
63 nominally known, uncertainties remain in terms of the total emission fluxes annually released
64 into the troposphere (Kuenen et al., 2014). Moreover, the measured OA load largely exceeds
65 the emitted POA fractions at most measurement sites around the world. A secondary fraction
66 (SOA), formed from the condensation of oxidized gases with low-volatility on pre-existing
67 particles, is found to be the dominant fraction of OA (Crippa et al., 2014; Huang et al., 2014;
68 Jimenez et al., 2009). Such low-volatility products are produced in the atmosphere when
69 higher volatility organic gases are oxidized by ozone (O_3), hydroxyl (OH) radical and/or
70 nitrate (NO_3) radical. The physical and chemical processes leading to the formation of SOA
71 are numerous, e.g. oxidation and condensation, oligomerization or aqueous-phase formation,
72 and they are very uncertain and currently under debate (Hallquist et al., 2009; Tsigaridis et
73 al., 2014; Fuzzi et al., 2015; Woody et al., 2016). Moreover, the solubility of organic
74 compounds in water is also a crucial parameter affecting the life time of organic particles and
75 gases in the atmosphere (Hodzic et al., 2016).

76 Available long-term measurements might help in elucidating the composition and origin of
77 OA in different seasons. Canonaco et al. (2015) presented direct evidence for significant
78 changes in the SOA fingerprint between summer and winter from 13 months of OA
79 measurements conducted in Zürich using the aerosol chemical speciation monitor (ACSM).
80 Their results indicate that summer oxygenated OA mainly arises from biogenic precursors
81 whereas winter oxygenated OA is more strongly influenced by wood burning emissions.
82 Moreover, numerous ambient studies with aircraft of open biomass burning plumes do not
83 show a net increase in OA, despite observed oxidation (Cubison et al., 2011; Jolleys et al.,
84 2012). It is therefore necessary that the chemical transport models (CTMs) correctly
85 reproduce OA concentrations by taking into account all the uncertainties and variability of
86 observations.

87 Most of the CTMs today account for SOA formation from biogenic and anthropogenic high
88 volatility precursors such as terpenes, isoprene, xylene and toluene which have a saturation
89 concentration (C^*) higher than $10^6 \mu\text{g m}^{-3}$ (Aksoyoglu et al., 2011; Ciarelli et al., 2016a). A
90 few models also include intermediate volatility organic compounds (IVOCs) with a C^* of 10^3
91 - $10^6 \mu\text{g m}^{-3}$ and semivolatile organic compounds (SVOCs) with a C^* of $0.1 - 10^3 \mu\text{g m}^{-3}$ co-

92 emitted with POA (Bergström et al., 2012; Ciarelli et al., 2016a; Denier van der Gon et al.,
93 2015; Fountoukis et al., 2014; Tsimpidi et al., 2010; Woody et al., 2016). In these
94 applications, the volatility distributions of POA and IVOCs emissions are based on the study
95 of Robinson et al. (2007), where the IVOC mass is assumed to be 1.5 times the total organic
96 mass available in the semivolatile range.

97 The standard gridded emission inventories do not yet include SVOCs and their emissions are
98 still highly uncertain as their measurement is strongly affected by the method used (Lipsky
99 and Robinson, 2006). A recent study by Denier van der Gon et al. (2015) reported a new
100 residential wood burning emission inventory including SVOCs, where emissions are higher
101 by a factor of 2-3 on average than those in the EUCAARI inventory (Kulmala et al., 2011).
102 The new emission inventory was used in two CTMs (EMEP and PMCAMx) and it improved
103 the model performance for the total OA (Denier van der Gon et al., 2015). Ciarelli et al.
104 (2016a) showed that allowing for evaporation of primary organic particles as available in the
105 European emission inventories degraded the model performance for the total OA mass
106 (further under-predicted OA but the POA to SOA ratio in a better agreement with
107 measurements). In the same study, on the other hand, model performance improved when
108 volatility distribution that implicitly accounts for missing semivolatile material (increasing
109 POA emissions by a factor of 3) was deployed.

110 Various modelling studies were performed by increasing POA emissions by a factor of 3 to
111 compensate for the missing gaseous emissions based on partitioning theory predictions
112 (Ciarelli et al., 2016a; Fountoukis et al., 2014; Shrivastava et al., 2011; Tsimpidi et al., 2010).
113 Fig. S1 shows the partitioning of $\sim 1 \mu\text{g m}^{-3}$ of POA at different temperatures using the latest
114 available volatility distribution for biomass burning (May et al., 2013). The ratio between the
115 available gas and particle phase material in the semivolatile range is predicted to be roughly 3.
116 This implies that, in these applications, the new emitted organic mass (POA + SVOCs +
117 IVOCs) is 7.5 times higher than in original emissions (i.e., $\text{OM} = (3*\text{POA}) + (1.5*(3*\text{POA}))$)
118 which could be used as an indirect method to account for missing organic material in the
119 absence of more detailed gridded emission inventories.

120 Along with ambient measurement studies, novel wood burning smog chamber studies provide
121 more insight into wood burning SOA formation and the nature of its precursors. Bruns et al.
122 (2016) performed several wood-burning aging experiments in a $\sim 7 \text{ m}^3$ smog chamber. Using
123 proton-transfer-reaction mass spectrometry (PTR-MS) they characterized SOA precursors at

124 the beginning of each aging experiment and found that up to 80% of the observed SOA could
125 be explained with a collection of a few SOA precursors that are usually not accounted in
126 regional CTMs (e.g. cresol, phenol, naphthalene). Recently, we used those chamber data to
127 parameterize a hybrid volatility basis set (Ciarelli et al., 2016b). The results provided new
128 direct information regarding the amount of wood burning SOA precursors which could be
129 directly used in CTM applications in the absence of more refined wood burning emissions in
130 gridded inventories. The box-model application reproduced the chamber data with an error of
131 approximately 25% on the OA mass and 15% on the O:C ratio (Ciarelli et al., 2016b).

132 In the current study, the updated volatility basis set (VBS) parameterization was implemented
133 in the comprehensive air quality model with extensions (CAMx) model, and simulations were
134 performed in Europe for a winter period in February-March 2009. Results are compared with
135 previous simulations using the original VBS framework (Ciarelli et al., 2016a) and with
136 source apportionment data at eleven sites with different exposure characteristics, obtained
137 using PMF applied to AMS measurements (Crippa et al., 2014).

138 **2 Method**

139 **2.1 Regional modelling with CAMx**

140 The CAMx version 5.41 with VBS scheme (ENVIRON, 2011; Koo et al., 2014) was used in this
141 study to simulate an EMEP measurement campaign between 25 February and 26 March 2009
142 in Europe. The modelling method and input data were the same as those used in the
143 EURODELTA III (ED III) project, described in detail in Ciarelli et al. (2016a). The model
144 domain covers Europe with a horizontal resolution of $0.25^\circ \times 0.25^\circ$. Meteorological
145 parameters were calculated from ECMWF IFS (Integrated Forecast System) data at 0.2°
146 resolution. There were 33 terrain-following σ -levels from ~20 m above ground level (first
147 layer) up to about 350 hPa, as in the original IFS data. For the gas phase chemistry, the
148 Carbon Bond (CB05) mechanism (Yarwood, 2005). The ISORROPIA thermodynamic model
149 (Nenes et al., 1998) was used for the partitioning of inorganic aerosols (sulfate, nitrate,
150 ammonium, sodium and chloride). Aqueous sulfate and nitrate formation in cloud water was
151 calculated using the RADM algorithm (Chang et al., 1987). Formation and evolution of OA is
152 treated with a hybrid volatility basis set (VBS) that accounts for changes in volatility and O:C
153 ratio (Koo et al., 2014) with dilution and aging. Particle size distributions were treated with a
154 two static mode scheme (fine and coarse). The results presented in this study refer to the fine

155 fraction (PM_{2.5}). We parameterized the biomass burning sets based on chamber data as
156 described in Ciarelli et al. (2016b).

157 The anthropogenic emission inventory was made available for the ED III community team by
158 the National Institute for Industrial Environment and Risks (INERIS) at 0.25° x 0.25°
159 horizontal resolution. More information regarding the anthropogenic emission inventories are
160 available in Bessagnet et al. (2014, 2016) and Ciarelli et al. (2016a). Hourly emissions of
161 biogenic VOCs, such as monoterpenes, isoprene, sesquiterpenes, xylene and toluene, were
162 calculated using the Model of Emissions of Gases and Aerosols from Nature MEGANv2.1
163 (Guenther et al., 2012) for each grid cell in the model domain.

164 **2.2 Organic aerosol scheme**

165 The biomass burning organic aerosol scheme was constrained using recently available wood
166 burning smog chamber data (Bruns et al., 2016) as described in Ciarelli et al. (2016b). The
167 model deploys three different basis sets (Donahue et al., 2011) to simulate the emissions of
168 organics from biomass burning and their evolution in the atmosphere. The first set allocates
169 fresh emissions into five volatility bins with saturation concentrations ranging between 10⁻¹
170 and 10³ µg m⁻³ following the volatility distribution and enthalpy of vaporization proposed by
171 May et al. (2013). In order to include gas-phase organics in the semivolatile range in the
172 absence of more detailed inventory data, we used the approach of increasing the standard
173 emissions by a factor of 3 proposed by previous studies (Shrivastava et al., 2011; Tsimpidi et
174 al., 2010) which is also in line with the recent European study on the revision of the
175 residential wood combustion emissions (Denier van der Gon et al., 2015). This approach of
176 including the semivolatile compounds can be used until detailed emission inventories with
177 more realistic inter-country distribution of the emissions become available (e.g. Denier van
178 der Gon et al., 2015). The second set allocates oxidation products from SVOCs after shifting
179 the volatility by one order of magnitude. The third set allocates oxidation products from the
180 traditional VOCs and biogenic precursors (xylene, toluene, isoprene, monoterpenes and
181 sesquiterpenes) and from non-traditional SOA precursors retrieved from chamber data (~4.75
182 times the amount of organic material in the semivolatile range, Ciarelli et al., 2016b). Primary
183 and secondary semivolatile compounds react with OH in the gas-phase with a rate constant of
184 4×10⁻¹¹ cm³ molec⁻¹ s⁻¹ (Donahue et al., 2013), which decreases their saturation concentration
185 by one order of magnitude. This implies that also aging of biogenic products is implicitly
186 taken into account.

187 A reaction rate of $4 \times 10^{-11} \text{cm}^3 \text{molec}^{-1} \text{s}^{-1}$ was also applied to the rest of the anthropogenic
188 sources (referred to as HOA) in order to be consistent among all the other anthropogenic
189 sources as already proposed by more recent studies for the range of saturation concentrations
190 used here (Donahue et al., 2013). No heterogeneous oxidation of organic particles or
191 oligomerization processes is included in the model. The new model parameterization
192 described in this study is referred to as VBS_BC_NEW throughout the paper to distinguish it
193 from the previous base case called VBS_BC as given in Ciarelli et al. (2016a). All the VBS
194 sets are listed in Table 1. More detailed on the VBS scheme can be found in Ciarelli et al.
195 (2016b) and Koo et al. (2014).

196 **2.3 Model evaluation**

197 The model results for the period between 25 February and 26 March 2009 were compared
198 with OA concentrations measured by AMS at 11 European sites. Modelled BBPOA, HOA
199 and SOA concentrations were compared with multi-linear engine 2 (ME-2) analysis
200 performed on AMS data (Paatero, 1999) using source finder (SoFi) (Canonaco et al., 2013;
201 Crippa et al., 2014). Elevated sites such as Montseny and Puy de Dôme were also included in
202 the analysis and modelled concentrations for these two sites were extracted from higher layers
203 in order to minimize the artefacts due to topography in a terrain-following coordinate system.
204 This was not the case in our previous application, where model OA concentrations were
205 extracted from the surface layer (Ciarelli et al., 2016a). We assumed OA emissions from
206 SNAP2 (emissions from non-industrial combustion plants in the Selected Nomenclature for
207 Air Pollution) and SNAP10 (emissions from agriculture, about 6% of POA in SNAP2), to be
208 representative of biomass burning emissions and thus comparable to the BBPOA PMF factor.
209 OA from all other SNAP categories were compared against HOA-like PMF factors.
210 Unfortunately, gridded emissions for SNAP2 include other emission sources (i.e., coal
211 burning which might be important in eastern European countries like Poland). We could not
212 resolve our emission inventory with sufficient detail to separate the contribution of coal for
213 these European sites (Crippa et al., 2014). Finally, the SOA fraction was compared to the
214 PMF-resolved oxygenated organic aerosol (OOA) fraction.

215 Statistics were reported in terms of mean bias (MB), mean error (ME), mean fractional bias
216 (MFB), mean fractional error (MFE) and coefficient of determination (R^2) (see Table S1 for
217 the definition of statistical parameters).

218 3 Results and discussions

219 3.1 Analysis of the modelled OA

220 Figure 1 shows the average modelled OA concentrations and surface temperature for the
221 period between 25 February and 26 March 2009. Temperatures were below 0°C in the north,
222 ranged 5-10°C in central Europe and were above 10°C in the southern part of the domain.
223 Model performance for surface temperature was evaluated within the ED III exercise and
224 found to be reproduced reasonably well, with a general under-prediction of around 1°C
225 (Bessagnet et al., 2014).

226 A clear spatial variability in the modelled OA concentrations is observed (Fig. 1). Predicted
227 OA concentrations were higher in eastern European countries (especially Romania and
228 southern Poland) as well as over northern Italy (8-10 $\mu\text{g m}^{-3}$ on average) whereas they were
229 lower in the northern part of the domain. A similar spatial distribution of OA concentrations
230 was also reported by Denier van der Gon et al. (2015) using the EMEP model. Relatively high
231 OA concentrations over the Mediterranean Sea are mainly of secondary origin due to
232 enhanced photochemical activity (more details are found in Section 3.2). In addition, the
233 reduced deposition efficiency over water leads to higher OA levels.

234 The scatter plots in Fig. 2 show the modelled (VBS_BC_NEW) versus measured daily
235 average OA concentrations at 11 sites in Europe together with the results from our previous
236 model application (VBS_BC, Ciarelli et al., 2016a) for comparison. The modified VBS
237 scheme (VBS_BC_NEW) predicts higher OA concentrations compared to our previous study
238 using the original scheme (VBS_BC) (~ 60% more OA on average at all sites). Statistical
239 parameters improved significantly (Table 2); the mean fractional bias MFB decreased from -
240 61% in VBS_BC to -29% in VBS_BC_NEW and the model performance criteria were met
241 (Boylan and Russell, 2006). The coefficient of determination remained almost unchanged for
242 OA in the VBS_BC_NEW case ($R^2=0.58$) compared to VBS_BC ($R^2=0.57$) indicating that the
243 original model was able to similarly capture the OA daily variation, but not its magnitude.
244 Improvements in the modelled SOA fraction were also observed using the original VBS
245 approach (Koo et al., 2014) when aging of the biomass burning vapours were taken into
246 account (Fig. S4). The majority of the stations show an $R^2 \geq 0.4$. Lower values were found for
247 the elevated sites of Montseny and Puy de Dome ($R^2=0.17$ and $R^2=0.13$, respectively) and
248 also at the Helsinki site ($R^2=0.06$). In spite of the improvements with respect to earlier studies,

249 modelled OA is still lower than measured (mean bias MB from $-0.1 \mu\text{g m}^{-3}$ up to $-3.1 \mu\text{g m}^{-3}$)
250 at most of the sites, with only a slight overestimation at a few locations (MB from $0.3 \mu\text{g m}^{-3}$
251 up to $0.9 \mu\text{g m}^{-3}$).

252 The observed OA gradient among the 11 sites was reproduced very well ($R^2 = 0.72$) (Fig. 3).
253 Both measured and modelled OA concentrations were highest in Barcelona. Other sites with
254 concentrations greater than $2 \mu\text{g m}^{-3}$ were Payerne, Helsinki, Vavihill and Montseny.
255 Barcelona and Helsinki are both classified as urban stations, which justifies the higher OA
256 loads due to the anthropogenic activities (e.g. traffic, cooking and heating). Anthropogenic
257 activities in the area of Barcelona could also affect OA concentrations at Montseny which is
258 about 40 km away. In the case of Payerne and Vavihill, the relatively high OA concentrations
259 might be due to residential heating, where wood is largely used as a combustion fuel during
260 cold periods (Denier van der Gon et al., 2015). For Chilbolton, located not far from London,
261 this might not be the case: the fuel wood usage in the UK is the lowest in Europe (Denier van
262 der Gon et al., 2015). Ots et al. (2016) suggested the possibility of missing diesel-related
263 IVOCs emissions, which might be an important source of SOA in those regions. However,
264 other studies reported substantial contribution from solid fuel combustion to OA (Young et
265 al., 2015). In this case, it might be that difficulties in reproducing the OA concentration are
266 mainly related to the relatively complex area of the site (i.e., close to the English Channel).
267 An evaluation of diurnal variations of HOA and SOA concentrations for this site showed a
268 consistent under-prediction of both components (Fig. S2).

269 **3.2 Analysis of the OA components**

270 The predicted POA spatial distribution (Fig. 4) resembles the residential heating emission
271 pattern of different countries (Bergström et al., 2012). The highest POA concentrations were
272 predicted in east European countries, France, Portugal and in northern Italy ($\sim 3\text{-}5 \mu\text{g m}^{-3}$)
273 whereas they were less than $1 \mu\text{g m}^{-3}$ in the rest of the model domain. Very low OA
274 concentrations in Sweden were already shown by previous European studies. Bergström et al.
275 (2012) reported that emissions of organic carbon (OC) from the residential heating sector in
276 Sweden were lower than those in Norway by a factor of 14 in spite of its higher wood usage
277 by 60%. This indicates an underestimation of emissions from residential heating in the
278 emission inventory. The spatial distribution of SOA concentrations, on the other hand, is more
279 widespread with a visible north to south gradient (Fig. 4). Higher SOA concentration were
280 predicted close to primary emission sources (e.g. Poland, Romania, Po Valley and Portugal)

281 but also in most of the countries below 50° latitude and over the Mediterranean Sea where
282 higher OH concentration, reduced deposition efficiency and high contribution from long-
283 range transport are expected (average concentrations around 3-4 $\mu\text{g m}^{-3}$).

284 Comparison of results from this study (VBS_BC_NEW) with the earlier one (VBS_BC,
285 Ciarelli et al., 2016a) suggests that the new VBS scheme predicts higher SOA concentrations
286 by about a factor of 3 (Fig. 5) and improves the model performance when comparing assessed
287 OOA from measurements with modelled SOA (Table 4). POA concentrations, on the other
288 hand, are clustered below 1 $\mu\text{g m}^{-3}$ except in Barcelona (Fig. 5), showing an $R^2=0.36$ (Table
289 3). Although predicted POA concentrations at Barcelona were lower than the measurements,
290 MFB=-47% and MFE=69% were still in the range for acceptable performance criteria (MFE
291 $\leq +75\%$ and $-60 < \text{MFB} < +60\%$, Boylan and Russell, 2006). On the other hand, the model
292 over-predicted the POA concentrations at Hyytiälä (MFB=131% and MFE=131%), Helsinki
293 (MFB=95% and MFE=100%) and Cabauw (MFB=76% and MFE=86%) mainly due to the
294 overestimated BBPOA fraction as seen in Fig. 6.

295 At most of the sites, OA was dominated by SOA (Fig. 6 and Fig. 7) which was
296 underestimated in particular at Chilbolton, Melpitz and Vavihill (Table 4). As already
297 mentioned, the under-prediction of SOA concentrations might be attributed to missing SOA
298 precursors or uncertainties in SOA formation mechanisms and removal processes. On the
299 other hand, the remote station of Mace Head showed a positive bias for SOA (MFB = 30%),
300 even though model and measurement concentrations were very similar (0.54 and 0.35 $\mu\text{g m}^{-3}$,
301 respectively), which could be attributed to an overestimated contribution from the boundaries.
302 The relatively small positive bias at the two elevated sites, Montseny and Puy de Dome (MFB
303 = 4% and 17%, respectively), is most likely the result of difficulties in capturing the inversion
304 layer, as confirmed by the over-prediction of other PM species at these sites (Fig. S3).

305 Mostly traffic-related HOA was underestimated at the urban site Barcelona (Table S2, Fig. 6),
306 with the model not able to reproduce the diurnal variation of HOA at this urban site likely due
307 to poorly reproduced meteorological conditions or too much dilution during day time in the
308 model (Fig. S2). The under-prediction of the HOA fraction is consistent with our previous
309 study where model evaluation for NO_2 revealed a systematic under-estimation of the
310 modelled concentration (Ciarelli et al., 2016a). The coarse resolution of the domain ($0.25^\circ \times$
311 0.25°) may result in too low emissions especially at urban sites. In addition, the gridded
312 emission inventories still represent a large source of uncertainties for CTM applications. The

313 majority of the NO_x (NO+NO₂) emissions in Europe arises from the transportation sector
314 (SNAP7), which might have much larger uncertainties than previously thought (Vaughan et
315 al., 2016). An evaluation of planetary boundary layer height (PBLH) within the EDIII shows
316 that although the PBLH was quite well represented in general in the ECMWF IFS
317 meteorological fields, CAMx tends to underestimate the night-time minima and to
318 overestimate some daytime peaks. The other urban site considered in this study is Helsinki. In
319 this case, HOA concentrations were over-predicted, as seen in Figs. 6 and S2, which might
320 indicate missing dispersion processes in the model or under-estimated dilution.

321 The modelled BBPOA fraction on the other hand was generally overpredicted as in our
322 previous application (Table S4), with an average MFB of 50% (Table S3, Figs. 6-7), which
323 might arise from various factors: 1) In the model, POA emissions from SNAP2 and SNAP10
324 are assumed to be representative of BBPOA emissions which might not be the case for all
325 European countries (other non-wood fuels such as coal, which is allocated to SNAP2 category
326 and could not be separated in this study), 2) The under-prediction of the modelled surface
327 temperature (Bessagnet et al., 2014) will directly influence the partitioning of organic material
328 in the semivolatile range, favouring freshly emitted organic material to condense more to the
329 particle phase, 3) Uncertainties in the adopted volatility distributions and/or in the oxidation
330 processes of semivolatile organic vapours, 4) The simplistic way of accounting for the
331 semivolatile part of primary emissions might lead, in some areas, to the double counting of
332 such compounds 5) Uncertainties in the retrieved BBPOA fraction from PMF analysis.

333 The temporal variability of OA concentrations was reproduced quite well (Fig. 8); the
334 magnitudes of only a few (Vavihill, Chilbolton and Barcelona) were underestimated. Diurnal
335 variations of HOA, BBPOA and SOA components at the rural-background sites suggest that
336 the model was able to reproduce the relatively flat profile of the measured SOA and the
337 increased BBPOA concentrations at night (Fig. 9). On the other hand, there was a slight
338 underestimation of HOA during the day, especially around noon, possibly as a result of too
339 much dilution in the model.

340 In our previous application, we performed a sensitivity study with increased biogenic and
341 residential heating emissions by a factor of two (Ciarelli et al., 2016a). While the model was
342 rather insensitive to the increased biogenic emissions during winter periods, a substantial
343 increase in the OA concentrations was observed when emissions from residential heating
344 were doubled. The model with doubled emissions from residential heating

345 (VBC_BC_2xBBOA), overestimated the POA fraction at most of the sites (Fig. 10) with
346 smaller effects on SOA, even though a better closure was achieved between modelled and
347 observed OA. The results of the simulations using the new parameterization
348 (VBC_BC_NEW), on the other hand, were closer to the measurement data especially for the
349 SOA fraction (Fig. 10).

350 **3.3 Residential versus non-residential combustion precursors**

351 More detailed source apportionment studies were performed in order to assess the importance
352 of residential and non-residential combustion precursors for OA and SOA. The upper panel in
353 Fig. 11 shows the relative contributions to SOA from residential and non-residential
354 combustion precursors. The model results indicate that non-residential combustion and
355 transportation precursors contribute to about 30-40 % of the SOA formation (with increasing
356 contribution at urban and near-industrialized sites) whereas residential combustion (mainly
357 related to wood burning) contributes to a larger extent, i.e., around 60-70%. The residential
358 combustion precursors were further apportioned to semivolatile and higher volatility
359 precursors (Fig. 11, lower panel). In particular, SVOC precursors exhibit a south-to-north
360 gradient with increasing contribution to the residential heating related OA for stations located
361 in the southern part of the domain (maximum and minimum contributions of 42 and 17% in
362 Montseny and Hyytiälä, respectively). Such a gradient also reflects the effect of temperature
363 on the partitioning of semivolatile organic material: the lower temperatures in the northern
364 part of the domain will reduce the saturation concentration of the organic compounds
365 allowing primary organic material to favour the particle phase and reducing the amount of
366 SVOCs available that could act as SOA precursors. In the southern part of the domain, where
367 more OH is available, the higher temperature will favour more organic material in the
368 semivolatile range to reside in the gas-phase, rendering it available for oxidation. On the other
369 hand, no south-to-north gradient was predicted for the SOA formed from the higher volatility
370 class of precursors. Source apportionment for different volatilities classes of the non-
371 residential and transportation sectors is currently not implemented for this model application.
372 Since biogenic SOA is included in the same set as the biomass burning (set3) for this model
373 application, we performed a sensitivity test with no SOA formation from biogenic precursors
374 (where the reactions of isoprene, monoterpene and sesquiterpene with OH, O₃ and NO₃ were
375 turned off). Our results indicated that for this period, biogenic precursors contribute to SOA to
376 a lesser extent (5-20%) than the anthropogenic ones, with higher contributions at southern

377 stations consistent with higher temperatures, and consequently more biogenic emissions
378 compared to the northern stations (Fig. S5). The most predominant source was still predicted
379 to be anthropogenic. Snow cover for March 2009 as retrieved from the TERRA/MODIS
380 revealed that larger parts of the Scandinavian countries were almost completely covered with
381 snow (Fig. S6), partially suppressing the emission of biogenic precursors and in line with very
382 low contribution predicted from biogenic sources in Helsinki and Hyytiälä. Comparison of
383 SOA from VBS_BC_NEW and the sensitivity test with no biogenic SOA formation showed
384 similar improvement with respect to VBS_BC, with differences occurring mainly in the
385 southern stations of Barcelona and Montseny (Fig. S7).

386 A comprehensive summary of the contribution to the total OA from all the sources (i.e. HOA,
387 BBPOA, residential combustion semivolatile precursors, residential combustion higher
388 volatility precursors and non-residential combustion precursors) is shown in Fig. 12 at each of
389 the measurement sites. Residential combustion precursors in the semivolatile range
390 contributed from 6 to 30% whereas higher volatility compounds contributed to a larger extent,
391 i.e. from 15 to 38%. SOA from non-residential combustion precursors contributed from 10 to
392 37% to the total OA. The primary sources HOA and BBPOA contributed from 3 to 30% and
393 1-39%, respectively. These results lead to the conclusion that the overall contribution of
394 residential combustion to OA concentrations in Europe varies between 52% at stations in the
395 UK and 75-76% at stations in Scandinavia.

396 **Conclusion**

397 This study aims to evaluate recent VBS parameterizations in commonly used CTMs and to
398 underline the importance of taking into account updated and more detailed SOA schemes as
399 new ambient and chamber measurements elucidate the high complexity and strong variability
400 of OA. In this context, a new VBS parameterization (based on recent wood burning
401 experiments) implemented in CAMx was evaluated against high-resolution AMS
402 measurements at 11 sites in Europe during February-March 2009, one of the winter EMEP
403 intensive measurement campaigns. Results obtained from this study were compared with
404 those from our earlier work in which the original VBS scheme in CAMx was applied. A
405 detailed source apportionment for the organic aerosol (OA) fraction was discussed. This study
406 provided the following outcome:

- 407 - A considerable improvement was found for the modelled OA concentrations
408 compared to our previous studies mainly due to the improved secondary organic

409 aerosol (SOA) performance. The average bias for the 11 AMS sites decreased by
410 about 60% although the model still underestimates the SOA fraction.

411 - Both model and PMF source apportionment based on measurements suggested that
412 OA was mainly of secondary origin with smaller primary contribution, with primary
413 contribution of 13 and 25% for HOA and BBPOA, respectively. Predicted HOA
414 concentrations were in the range of those retrieved from the PMF analysis at most of
415 the sites except at the urban Barcelona site which could be related to the uncertainties
416 in emissions or too much dilution in the model. On the other hand, the modelled
417 BBPOA was higher than the measurements at several stations indicating the need for
418 further studies on residential heating emissions, their volatility distribution and
419 oxidation pathway of the semivolatile organic gases. In addition, more detailed
420 emission inventories are needed to characterize the semivolatile components better, as
421 proposed by Denier van der Gon et al. (2015).

422 - Emissions from the residential heating sector (SNAP2) largely influenced the OA
423 composition. The modeled primary BBPOA fraction contributed from 46% to 77% of
424 the total primary organic fraction (POA), with an average contribution of 65%. Non-
425 residential combustion and transportation precursors contributed about 30-40% to
426 SOA (with increasing contribution at urban and near-industrialized sites) whereas
427 residential combustion (mainly related to wood burning) contributes to a larger extent,
428 ~ 60-70%. Moreover, the contribution to OA from residential combustion precursors
429 in different range of volatilities was also investigated: residential combustion gas-
430 phase precursors in the semivolatile range contributed from 6 to 30% with a positive
431 south-to-north gradient. On the other hand, higher volatility residential combustion
432 precursors contributed from 15 to 38% showing no specific gradient among the
433 stations.

434 - Model simulations performed with and without biogenic SOA formation revealed that,
435 for this period, biogenic SOA contributed only to a small extent to the total SOA (5-
436 20%), with an increasing gradient from north to south.

437

438

439 **Acknowledgements**

440 We thank the EURODELTA III modelling community, especially INERIS, TNO as well as
441 ECMWF for providing various model input data. Calculations of land use data were
442 performed at the Swiss National Supercomputing Centre (CSCS). We thank D. Oderbolz for
443 developing the CAMxRunner framework to ensure reproducibility and data quality among the
444 simulations and sensitivity tests. M. Tinguely for the visualization software, and RAMBOLL
445 ENVIRON for their valuable comments. This study was financially supported by the Swiss
446 Federal Office of Environment (FOEN). The research leading to these results received
447 funding from the European Community's Seventh Framework Programme (FP7/2007-2013)
448 under grant agreement no. 290605 (PSI-FELLOW), from the Competence Center
449 Environment and Sustainability (CCES) (project OPTIWARES) and from the Swiss National
450 Science Foundation (WOOSHI grant 140590). We thank D.A. Day for analysis on the
451 DAURE dataset. Erik Swietlicki for the Vavihill dataset, Claudia Mohr for the Barcelona
452 dataset, A. Kiendler-Scharr for Cabauw AMS data, Eriko Nemitz for the Chilboton data,
453 Karine Sellegri for the Puy de Dôme dataset and Jose-Luis Jimenez for the measurements data
454 in Montseny. The AMS measurements were funded through the European EUCAARI IP. We
455 would like to acknowledge EMEP for the measurement data used here, HEA-PRTL14, EPA
456 Ireland, and the Science Foundation Ireland for facilitating measurements at Mace Head.

457

458

459

460

461

462

463

464

465

466

467

468 **References**

469 Aksoyoglu, S., Keller, J., Barmadimos, I., Oderbolz, D., Lanz, V. A., Prévôt, A. S. H. and
470 Baltensperger, U.: Aerosol modelling in Europe with a focus on Switzerland during summer
471 and winter episodes, *Atmos. Chem. Phys.*, 11 (14), 7355–7373, doi:10.5194/acp-11-7355-
472 2011, 2011.

473 Bergström, R., Denier van der Gon, H. A. C., Prévôt, A. S. H., Yttri, K. E. and Simpson, D.:
474 Modelling of organic aerosols over Europe (2002–2007) using a volatility basis set (VBS)
475 framework: application of different assumptions regarding the formation of secondary organic
476 aerosol, *Atmos. Chem. Phys.*, 12 (18), 8499–8527, doi:10.5194/acp-12-8499-2012, 2012.

477 Bessagnet, B., Colette, A., Meleux, F., Rouïl, L., Ung, A., Favez, O., Cuvelier, C., Thunis, P.,
478 Tsyro, S., Stern, R., Manders, A., Kranenburg, R., Aulinger, A., Bieser, J., Mircea, M.,
479 Briganti, A., Cappelletti, A., Calori, G., Finardi, S., Silibello, C., Ciarelli, G., Aksoyoglu, S.,
480 Prévôt, A., Pay, M. T., Baldasano, J. M., García Vivanco, M., Garrido, J. L., Palomino, I.,
481 Martín, F., Pirovano, G., Roberts, P., Gonzalez, L., White, L., Menut, L., Dupont, J. C.,
482 Carnevale, C. and Pederzoli, A.: The EURODELTA III exercise – Model evaluation with
483 observations issued from the 2009 EMEP intensive period and standard measurements in
484 Feb/Mar 2009, 2014.

485 Boylan, J. W. and Russell, A. G.: PM and light extinction model performance metrics, goals,
486 and criteria for three-dimensional air quality models, *Atmos. Environ.*, 40 (26), 4946–4959,
487 doi:10.1016/j.atmosenv.2005.09.087, 2006.

488 Bruns, E. A., El Haddad, I., Slowik, J. G., Kilic, D., Klein, F., Baltensperger, U. and Prévôt,
489 A. S. H.: Identification of significant precursor gases of secondary organic aerosols from
490 residential wood combustion, *Sci. Rep.*, 6, 27881, doi:10.1038/srep27881, 2016.

491 Canonaco, F., Crippa, M., Slowik, J. G., Baltensperger, U. and Prévôt, A. S. H.: SoFi, an
492 IGOR-based interface for the efficient use of the generalized multilinear engine (ME-2) for
493 the source apportionment: ME-2 application to aerosol mass spectrometer data, *Atmos. Meas.*
494 *Tech.*, 6 (12), 3649–3661, doi:10.5194/amt-6-3649-2013, 2013.

495 Canonaco, F., Slowik, J. G., Baltensperger, U. and Prévôt, A. S. H.: Seasonal differences in
496 oxygenated organic aerosol composition: implications for emissions sources and factor
497 analysis, *Atmos. Chem. Phys.*, 15 (12), 6993–7002, doi:10.5194/acp-15-6993-2015, 2015.

498 Chang, J. S., Brost, R. A., Isaksen, I. S. A., Madronich, S., Middleton, P., Stockwell, W. R.
499 and Walcek, C. J.: A three-dimensional Eulerian acid deposition model: Physical concepts

500 and formulation, *J. Geophys. Res. Atmospheres*, 92 (D12), 14681–14700,
501 doi:10.1029/JD092iD12p14681, 1987.

502 Ciarelli, G., Aksoyoglu, S., Crippa, M., Jimenez, J.-L., Nemitz, E., Sellegri, K., Äijälä, M.,
503 Carbone, S., Mohr, C., O'Dowd, C., Poulain, L., Baltensperger, U. and Prévôt, A. S. H.:
504 Evaluation of European air quality modelled by CAMx including the volatility basis set
505 scheme, *Atmos. Chem. Phys.*, 16 (16), 10313–10332, doi:10.5194/acp-16-10313-2016,
506 2016a.

507 Ciarelli, G., El Haddad, I., Bruns, E., Aksoyoglu, S., Möhler, O., Baltensperger, U. and
508 Prévôt, A. S. H.: Constraining a hybrid volatility basis set model for aging of wood burning
509 emissions using smog chamber experiments, *Geosci. Model Dev.*, accepted, 2016b.

510 Crippa, M., Canonaco, F., Lanz, V. A., Äijälä, M., Allan, J. D., Carbone, S., Capes, G.,
511 Ceburnis, D., Dall'Osto, M., Day, D. A., DeCarlo, P. F., Ehn, M., Eriksson, A., Freney, E.,
512 Hildebrandt Ruiz, L., Hillamo, R., Jimenez, J. L., Junninen, H., Kiendler-Scharr, A.,
513 Kortelainen, A.-M., Kulmala, M., Laaksonen, A., Mensah, A. A., Mohr, C., Nemitz, E.,
514 O'Dowd, C., Ovadnevaite, J., Pandis, S. N., Petäjä, T., Poulain, L., Saarikoski, S., Sellegri,
515 K., Swietlicki, E., Tiitta, P., Worsnop, D. R., Baltensperger, U. and Prévôt, A. S. H.: Organic
516 aerosol components derived from 25 AMS data sets across Europe using a consistent ME-2
517 based source apportionment approach, *Atmos. Chem. Phys.*, 14 (12), 6159–6176,
518 doi:10.5194/acp-14-6159-2014, 2014.

519 Cubison, M. J., Ortega, A. M., Hayes, P. L., Farmer, D. K., Day, D., Lechner, M. J., Brune,
520 W. H., Apel, E., Diskin, G. S., Fisher, J. A., Fuelberg, H. E., Hecobian, A., Knapp, D. J.,
521 Mikoviny, T., Riemer, D., Sachse, G. W., Sessions, W., Weber, R. J., Weinheimer, A. J.,
522 Wisthaler, A. and Jimenez, J. L.: Effects of aging on organic aerosol from open biomass
523 burning smoke in aircraft and laboratory studies, *Atmos. Chem. Phys.*, 11 (23), 12049–12064,
524 doi:10.5194/acp-11-12049-2011, 2011.

525 Denier van der Gon, H. A. C., Bergström, R., Fountoukis, C., Johansson, C., Pandis, S. N.,
526 Simpson, D. and Visschedijk, A. J. H.: Particulate emissions from residential wood
527 combustion in Europe – revised estimates and an evaluation, *Atmos. Chem. Phys.*, 15 (11),
528 6503–6519, doi:10.5194/acp-15-6503-2015, 2015.

529 Donahue, N. M., Epstein, S. A., Pandis, S. N. and Robinson, A. L.: A two-dimensional
530 volatility basis set: 1. organic-aerosol mixing thermodynamics, *Atmos. Chem. Phys.*, 11 (7),
531 3303–3318, doi:10.5194/acp-11-3303-2011, 2011.

532 Donahue, N. M., Chuang, W., Epstein, S. A., Kroll, J. H., Worsnop, D. R., Robinson, A. L.,
533 Adams, P. J. and Pandis, S. N.: Why do organic aerosols exist? Understanding aerosol
534 lifetimes using the two-dimensional volatility basis set, *Environ. Chem.*, 10 (3), 151,
535 doi:10.1071/EN13022, 2013.

536 ENVIRON: User's Guide, Comprehensive Air Quality Model with Extensions (CAMx),
537 Version 5.40, Environ International Corporation, California, 2011.

538 Fountoukis, C., Megaritis, A. G., Skyllakou, K., Charalampidis, P. E., Pilinis, C., Denier van
539 der Gon, H. A. C., Crippa, M., Canonaco, F., Mohr, C., Prévôt, A. S. H., Allan, J. D., Poulain,
540 L., Petäjä, T., Tiitta, P., Carbone, S., Kiendler-Scharr, A., Nemitz, E., O'Dowd, C., Swietlicki,
541 E. and Pandis, S. N.: Organic aerosol concentration and composition over Europe: insights
542 from comparison of regional model predictions with aerosol mass spectrometer factor
543 analysis, *Atmos. Chem. Phys.*, 14 (17), 9061–9076, doi:10.5194/acp-14-9061-2014, 2014.

544 Grieshop, A. P., Logue, J. M., Donahue, N. M. and Robinson, A. L.: Laboratory investigation
545 of photochemical oxidation of organic aerosol from wood fires 1: measurement and
546 simulation of organic aerosol evolution, *Atmos. Chem. Phys.*, 9 (4), 1263–1277,
547 doi:10.5194/acp-9-1263-2009, 2009.

548 Guenther, A. B., Jiang, X., Heald, C. L., Sakulyanontvittaya, T., Duhl, T., Emmons, L. K. and
549 Wang, X.: The Model of Emissions of Gases and Aerosols from Nature version 2.1
550 (MEGAN2.1): an extended and updated framework for modeling biogenic emissions, *Geosci.*
551 *Model Dev.*, 5 (6), 1471–1492, doi:10.5194/gmd-5-1471-2012, 2012.

552 Hallquist, M., Wenger, J. C., Baltensperger, U., Rudich, Y., Simpson, D., Claeys, M.,
553 Dommen, J., Donahue, N. M., George, C., Goldstein, A. H., Hamilton, J. F., Herrmann, H.,
554 Hoffmann, T., Iinuma, Y., Jang, M., Jenkin, M. E., Jimenez, J. L., Kiendler-Scharr, A.,
555 Maenhaut, W., McFiggans, G., Mentel, T. F., Monod, A., Prévôt, A. S. H., Seinfeld, J. H.,
556 Surratt, J. D., Szmigielski, R. and Wildt, J.: The formation, properties and impact of
557 secondary organic aerosol: current and emerging issues, *Atmos. Chem. Phys.*, 9 (14), 5155–
558 5236, doi:10.5194/acp-9-5155-2009, 2009.

559 Heald, C. L., Kroll, J. H., Jimenez, J. L., Docherty, K. S., DeCarlo, P. F., Aiken, A. C., Chen,
560 Q., Martin, S. T., Farmer, D. K. and Artaxo, P.: A simplified description of the evolution of
561 organic aerosol composition in the atmosphere, *Geophys. Res. Lett.*, 37 (8), n/a-n/a,
562 doi:10.1029/2010GL042737, 2010.

563 Hodzic, A., Kasibhatla, P. S., Jo, D. S., Cappa, C. D., Jimenez, J. L., Madronich, S., and Park,
564 R. J.: Rethinking the global secondary organic aerosol (SOA) budget: stronger production,
565 faster removal, shorter lifetime, *Atmos. Chem. Phys.*, 16, 7917-7941, doi:10.5194/acp-16-
566 7917-2016, 2016.

567 Huang, R.-J., Zhang, Y., Bozzetti, C., Ho, K.-F., Cao, J.-J., Han, Y., Daellenbach, K. R.,
568 Slowik, J. G., Platt, S. M., Canonaco, F., Zotter, P., Wolf, R., Pieber, S. M., Bruns, E. A.,
569 Crippa, M., Ciarelli, G., Piazzalunga, A., Schwikowski, M., Abbaszade, G., Schnelle-Kreis,
570 J., Zimmermann, R., An, Z., Szidat, S., Baltensperger, U., Haddad, I. E. and Prévôt, A. S. H.:
571 High secondary aerosol contribution to particulate pollution during haze events in China,
572 *Nature*, 514 (7521), 218–222, doi:10.1038/nature13774, 2014.

573 Jimenez, J. L., Canagaratna, M. R., Donahue, N. M., Prevot, A. S. H., Zhang, Q., Kroll, J. H.,
574 DeCarlo, P. F., Allan, J. D., Coe, H., Ng, N. L., Aiken, A. C., Docherty, K. S., Ulbrich, I. M.,
575 Grieshop, A. P., Robinson, A. L., Duplissy, J., Smith, J. D., Wilson, K. R., Lanz, V. A.,
576 Hueglin, C., Sun, Y. L., Tian, J., Laaksonen, A., Raatikainen, T., Rautiainen, J., Vaattovaara,
577 P., Ehn, M., Kulmala, M., Tomlinson, J. M., Collins, D. R., Cubison, M. J., Dunlea, E. J.,
578 Huffman, J. A., Onasch, T. B., Alfarra, M. R., Williams, P. I., Bower, K., Kondo, Y.,
579 Schneider, J., Drewnick, F., Borrmann, S., Weimer, S., Demerjian, K., Salcedo, D., Cottrell,
580 L., Griffin, R., Takami, A., Miyoshi, T., Hatakeyama, S., Shimono, A., Sun, J. Y., Zhang, Y.
581 M., Dzepina, K., Kimmel, J. R., Sueper, D., Jayne, J. T., Herndon, S. C., Trimborn, A. M.,
582 Williams, L. R., Wood, E. C., Middlebrook, A. M., Kolb, C. E., Baltensperger, U. and
583 Worsnop, D. R.: Evolution of organic aerosols in the atmosphere, *Science*, 326 (5959), 1525–
584 1529, doi:10.1126/science.1180353, 2009.

585 Jolleys, M. D., Coe, H., McFiggans, G., Capes, G., Allan, J. D., Crosier, J., Williams, P. I.,
586 Allen, G., Bower, K. N., Jimenez, J. L., Russell, L. M., Grutter, M. and Baumgardner, D.:
587 Characterizing the Aging of Biomass Burning Organic Aerosol by Use of Mixing Ratios: A
588 Meta-analysis of Four Regions, *Environ. Sci. Technol.*, 46 (24), 13093–13102,
589 doi:10.1021/es302386v, 2012.

590 Koo, B., Knipping, E. and Yarwood, G.: 1.5-Dimensional volatility basis set approach for
591 modeling organic aerosol in CAMx and CMAQ, *Atmos. Environ.*, 95, 158–164,
592 doi:10.1016/j.atmosenv.2014.06.031, 2014.

593 Kuenen, J. J. P., Visschedijk, A. J. H., Jozwicka, M. and Denier van der Gon, H. A. C.: TNO-
594 MACC_II emission inventory; a multi-year (2003–2009) consistent high-resolution European
595 emission inventory for air quality modelling, *Atmos. Chem. Phys.*, 14 (20), 10963–10976,
596 doi:10.5194/acp-14-10963-2014, 2014.

597 Kulmala, M., Asmi, A., Lappalainen, H. K., Baltensperger, U., Brenguier, J.-L., Facchini, M.
598 C., Hansson, H.-C., Hov, Ø., O’Dowd, C. D., Pöschl, U., Wiedensohler, A., Boers, R.,
599 Boucher, O., de Leeuw, G., Denier van der Gon, H. A. C., Feichter, J., Krejci, R., Laj, P.,
600 Lihavainen, H., Lohmann, U., McFiggans, G., Mentel, T., Pilinis, C., Riipinen, I., Schulz, M.,
601 Stohl, A., Swietlicki, E., Vignati, E., Alves, C., Amann, M., Ammann, M., Arabas, S., Artaxo,
602 P., Baars, H., Beddows, D. C. S., Bergström, R., Beukes, J. P., Bilde, M., Burkhardt, J. F.,
603 Canonaco, F., Clegg, S. L., Coe, H., Crumeyrolle, S., D’Anna, B., Decesari, S., Gilardoni, S.,
604 Fischer, M., Fjaeraa, A. M., Fountoukis, C., George, C., Gomes, L., Halloran, P., Hamburger,
605 T., Harrison, R. M., Herrmann, H., Hoffmann, T., Hoose, C., Hu, M., Hyvärinen, A., Hörrak,
606 U., Iinuma, Y., Iversen, T., Josipovic, M., Kanakidou, M., Kiendler-Scharr, A., Kirkevåg, A.,
607 Kiss, G., Klimont, Z., Kolmonen, P., Komppula, M., Kristjánsson, J.-E., Laakso, L.,
608 Laaksonen, A., Labonnote, L., Lanz, V. A., Lehtinen, K. E. J., Rizzo, L. V., Makkonen, R.,
609 Manninen, H. E., McMeeking, G., Merikanto, J., Minikin, A., Mirme, S., Morgan, W. T.,
610 Nemitz, E., O’Donnell, D., Panwar, T. S., Pawlowska, H., Petzold, A., Pienaar, J. J., Pio, C.,
611 Plass-Duelmer, C., Prévôt, A. S. H., Pryor, S., Reddington, C. L., Roberts, G., Rosenfeld, D.,
612 Schwarz, J., Seland, Ø., et al.: General overview: European Integrated project on Aerosol
613 Cloud Climate and Air Quality interactions (EUCAARI) – integrating aerosol research from
614 nano to global scales, *Atmos. Chem. Phys.*, 11, 13061–13143, doi:10.5194/acp-11-13061-
615 2011, 2011.

616 Lipsky, E. M. and Robinson, A. L.: Effects of Dilution on Fine Particle Mass and Partitioning
617 of Semivolatile Organics in Diesel Exhaust and Wood Smoke, *Environ. Sci. Technol.*, 40 (1),
618 155–162, doi:10.1021/es050319p, 2006.

619 May, A. A., Levin, E. J. T., Hennigan, C. J., Riipinen, I., Lee, T., Collett, J. L., Jimenez, J. L.,
620 Kreidenweis, S. M. and Robinson, A. L.: Gas-particle partitioning of primary organic aerosol

621 emissions: 3. Biomass burning, *J. Geophys. Res. Atmospheres*, 118 (19), 2013JD020286,
622 doi:10.1002/jgrd.50828, 2013.

623 Nenes, A., Pandis, S. N. and Pilinis, C.: ISORROPIA: a new thermodynamic equilibrium
624 model for multiphase multicomponent inorganic aerosols, *Aquat. Geochem.*, 4, 123–152,
625 1998, *Aquat. Geochem.*, 4, 123–152, 1998.

626 Ots, R., Young, D. E., Vieno, M., Xu, L., Dunmore, R. E., Allan, J. D., Coe, H., Williams, L.
627 R., Herndon, S. C., Ng, N. L., Hamilton, J. F., Bergström, R., Di Marco, C., Nemitz, E.,
628 Mackenzie, I. A., Kuenen, J. J. P., Green, D. C., Reis, S. and Heal, M. R.: Simulating
629 secondary organic aerosol from missing diesel-related intermediate-volatility organic
630 compound emissions during the Clean Air for London (ClearfLo) campaign, *Atmos. Chem.*
631 *Phys.*, 16 (10), 6453–6473, doi:10.5194/acp-16-6453-2016, 2016.

632 Paatero, P.: The Multilinear Engine: A Table-Driven, Least Squares Program for Solving
633 Multilinear Problems, including the n-Way Parallel Factor Analysis Model, *J. Comput.*
634 *Graph. Stat.*, 8 (4), 854, doi:10.2307/1390831, 1999.

635 Robinson, A. L., Donahue, N. M., Shrivastava, M. K., Weitkamp, E. A., Sage, A. M.,
636 Grieshop, A. P., Lane, T. E., Pierce, J. R. and Pandis, S. N.: Rethinking Organic Aerosols:
637 Semivolatile Emissions and Photochemical Aging, *Science*, 315 (5816), 1259–1262,
638 doi:10.1126/science.1133061, 2007.

639 Shrivastava, M., Fast, J., Easter, R., Gustafson Jr., W. I., Zaveri, R. A., Jimenez, J. L., Saide,
640 P. and Hodzic, A.: Modeling organic aerosols in a megacity: comparison of simple and
641 complex representations of the volatility basis set approach, *Atmos. Chem. Phys.*, 11, 6639–
642 6662, 2011.

643 Tsigaridis, K., Daskalakis, N., Kanakidou, M., Adams, P. J., Artaxo, P., Bahadur, R.,
644 Balkanski, Y., Bauer, S. E., Bellouin, N., Benedetti, A., Bergman, T., Berntsen, T. K.,
645 Beukes, J. P., Bian, H., Carslaw, K. S., Chin, M., Curci, G., Diehl, T., Easter, R. C., Ghan, S.
646 J., Gong, S. L., Hodzic, A., Hoyle, C. R., Iversen, T., Jathar, S., Jimenez, J. L., Kaiser, J. W.,
647 Kirkevåg, A., Koch, D., Kokkola, H., Lee, Y. H., Lin, G., Liu, X., Luo, G., Ma, X., Mann, G.
648 W., Mihalopoulos, N., Morcrette, J.-J., Müller, J.-F., Myhre, G., Myriokefalitakis, S., Ng, N.
649 L., O'Donnell, D., Penner, J. E., Pozzoli, L., Pringle, K. J., Russell, L. M., Schulz, M., Sciare,
650 J., Seland, Ø., Shindell, D. T., Sillman, S., Skeie, R. B., Spracklen, D., Stavrakou, T.,
651 Steenrod, S. D., Takemura, T., Tiitta, P., Tilmes, S., Tost, H., van Noije, T., van Zyl, P. G.,

652 von Salzen, K., Yu, F., Wang, Z., Wang, Z., Zaveri, R. A., Zhang, H., Zhang, K., Zhang, Q.
653 and Zhang, X.: The AeroCom evaluation and intercomparison of organic aerosol in global
654 models, *Atmos. Chem. Phys.*, 14 (19), 10845–10895, doi:10.5194/acp-14-10845-2014, 2014.

655 Tsimpidi, A. P., Karydis, V. A., Zavala, M., Lei, W., Molina, L., Ulbrich, I. M., Jimenez, J. L.
656 and Pandis, S. N.: Evaluation of the volatility basis-set approach for the simulation of organic
657 aerosol formation in the Mexico City metropolitan area, *Atmos. Chem. Phys.*, 10, 525–546,
658 2010.

659 Vaughan, A. R., Lee, J. D., Misztal, P. K., Metzger, S., Shaw, M. D., Lewis, A. C., Purvis, R.
660 M., Carslaw, D. C., Goldstein, A. H., Hewitt, C. N., Davison, B., Beevers, S. D. and Karl, T.
661 G.: Spatially resolved flux measurements of NO_x from London suggest significantly higher
662 emissions than predicted by inventories, *Faraday Discuss*, doi:10.1039/C5FD00170F, 2016.

663 Woody, M. C., Baker, K. R., Hayes, P. L., Jimenez, J. L., Koo, B. and Pye, H. O. T.:
664 Understanding sources of organic aerosol during CalNex-2010 using the CMAQ-VBS,
665 *Atmos. Chem. Phys.*, 16 (6), 4081–4100, doi:10.5194/acp-16-4081-2016, 2016.

666 Yarwood, G.: Updates to the Carbon Bond Chemical 852 Mechanism: CB05, 2005.

667 Young, D. E., Allan, J. D., Williams, P. I., Green, D. C., Flynn, M. J., Harrison, R. M., Yin,
668 J., Gallagher, M. W. and Coe, H.: Investigating the annual behaviour of submicron secondary
669 inorganic and organic aerosols in London, *Atmos. Chem. Phys.*, 15 (11), 6351–6366,
670 doi:10.5194/acp-15-6351-2015, 2015.

671

672

673 **4 Tables and Figures**

674 Table 1. Properties of the VBS space. Oxygen numbers for each volatility bin were calculated
 675 using the group-contribution of Donahue et al. (2011). Hydrogen numbers were calculated
 676 from the van Krevelen relation (Heald et al., 2010).

	log (C*)	Oxygen number	Carbon number	Hydrogen number	Molecular weight
POA set1*	-1	4.11	11.00	17.89	216
(BBOA-like)	0	3.43	11.75	20.07	216
Primary biomass	1	2.73	12.50	22.27	216
burning (BBPOA)	2	2.01	13.25	24.49	216
	3	1.27	14.00	26.73	215
SOA set2*	-1	4.53	9.00	13.47	194
(BBOA-like)	0	4.00	9.25	14.50	189
SOA from SVOCs	1	3.40	9.50	15.60	184
biomass burning	2	2.83	9.75	16.67	179
SOA set3*	-1	5.25	5.00	4.75	149
(BBOA-like)	0	4.70	5.25	5.80	144
SOA from	1	4.20	5.50	6.80	140
VOC/IVOCs biomass	2	3.65	5.75	7.85	135
burning and biogenics	3	3.15	6.00	8.85	131
POA set1**	-1	2.69	17.00	31.3	278
(HOA-like)	0	2.02	17.50	33.0	275
Rest of primary	1	1.34	18.00	34.7	272
anthropogenic sources	2	0.63	18.50	36.4	268
	3	0.0	19.00	38.0	266
SOA set1**	-1	4.90	7.00	9.10	172
(HOA-like)	0	4.38	7.25	10.1	167
SOA from rest of all	1	3.84	7.50	11.2	163
anthropogenic in all	2	3.30	7.75	12.2	158

volatility range (SVOCs,IVOCs,VOCs)	3	2.74	8.00	13.3	153
--	---	------	------	------	-----

677

678 *Based on Ciarelli et al. (2016b).

679 **Molecular structure as in Koo et al. (2014) and Ciarelli et al. (2016a).

680

681 Table 2. Statistics of OA for the VBS_BC_NEW case for February-March 2009 at each AMS
682 site as well as an average of all sites for both VBS_BC_NEW and VBS_BC. Bold numbers
683 represent the stations where model performance criteria were met.

Site*	Mean observed OA ($\mu\text{g m}^{-3}$)	Mean modelled OA ($\mu\text{g m}^{-3}$)	MB ($\mu\text{g m}^{-3}$)	ME ($\mu\text{g m}^{-3}$)	MFB [-]	MFE [-]	r	R ²
Barcelona (BCN)	8.3	5.1	-3.1	3.7	-0.4	0.5	0.6	0.4
Cabauw (CBW)	1.2	1.5	0.3	0.7	0.1	0.5	0.7	0.4
Chilbolton (CHL)	2.4	1.0	-1.4	1.5	-0.9	0.9	0.8	0.6
Helsinki (HEL)	2.7	3.6	0.9	1.8	0.3	0.6	0.3	0.1
Hyytiälä (SMR)	1.3	1.7	0.3	0.8	-0.1	0.6	0.8	0.6
Mace Head (MHD)	0.8	0.7	-0.1	0.3	-0.1	0.7	0.7	0.5
Melpitz (MPZ)	1.5	0.8	-0.6	0.9	-0.6	0.7	0.6	0.3
Montseny (MSY)	3.1	3.5	0.4	2.0	0.1	0.6	0.4	0.1
Payenne (PAY)	4.1	2.9	-1.2	1.9	-0.5	0.7	0.7	0.4
Puy de Dôme (PDD)	0.6	1.1	0.4	0.8	0.3	0.8	0.4	0.2
Vavihill (VAV)	3.9	2.1	-1.8	2.0	-0.8	0.8	0.8	0.6
VBS_BC_NEW	3.0	2.3	-0.7	1.6	-0.3	0.7	0.8	0.6
VBS_BC (Ciarelli et al., 2016a)	3.0	1.4	-1.5	1.8	-0.6	0.8	0.8	0.6

684 * Model OA concentrations extracted at surface level except for the stations of Puy de Dôme
 685 and Montseny.

686

687 Table 3. Statistics of POA for the VBS_BC_NEW case for February-March 2009 at each
 688 AMS site as well as an average of all sites for both VBS_BC_NEW and VBS_BC. Bold
 689 numbers represent the stations where model performance criteria were met.

Site	Mean observed POA ($\mu\text{g m}^{-3}$)	Mean modelled POA ($\mu\text{g m}^{-3}$)	MB ($\mu\text{g m}^{-3}$)	ME ($\mu\text{g m}^{-3}$)	MFB [-]	MFE [-]	r	R ²
Barcelona	4.0	2.0	-2.1	2.4	-0.5	0.7	0.4	0.2
Cabauw	0.4	0.9	0.5	0.5	0.8	0.9	0.5	0.2
Chilbolton	1.0	0.5	-0.5	0.5	-0.6	0.7	0.8	0.6
Helsinki	0.8	2.5	1.7	1.7	1.0	1.0	0.2	0.0
Hyytiälä	0.1	0.5	0.4	0.4	1.3	1.3	0.5	0.3
Mace Head	0.2	0.1	-0.1	0.2	0.5	1.0	0.2	0.1
Melpitz	0.3	0.3	0.1	0.2	0.3	0.7	0.5	0.2
Montseny	0.5	0.4	0.0	0.3	0.2	0.7	0.3	0.1
Payerne	0.7	1.1	0.3	0.6	0.5	0.7	0.5	0.3
Puy de Dôme	0.2	0.3	0.1	0.2	0.5	0.9	0.2	0.1
Vavihill	1.1	1.0	-0.1	0.6	-0.3	0.7	0.5	0.2
VBS_BC_NEW	0.9	0.9	-0.1	0.7	0.3	0.8	0.6	0.3
VBS_BC (Ciarelli et al., 2016a)	0.9	0.9	0.0	0.8	0.3	0.8	0.6	0.4

690

691

692

693

694

695

696 Table 4. Statistics of SOA for the VBS_BC_NEW case for February-March 2009 at each
 697 AMS site as well as an average of all sites for both VBS_BC_NEW and VBS_BC. Bold
 698 number represents the stations where model performance criteria were met.

Site	Mean observed SOA ($\mu\text{g m}^{-3}$)	Mean modelled SOA ($\mu\text{g m}^{-3}$)	MB ($\mu\text{g m}^{-3}$)	ME ($\mu\text{g m}^{-3}$)	MFB [-]	MFE [-]	r	R ²
Barcelona	4.4	3.2	-1.2	1.6	-0.4	0.5	0.7	0.5
Cabauw	1.0	0.6	-0.4	0.6	-0.7	0.9	0.7	0.4
Chilbolton	1.4	0.5	-0.9	1.0	-1.1	1.2	0.7	0.5
Helsinki	1.8	1.1	-0.7	1.1	-0.7	0.9	0.4	0.2
Hyytiälä	1.2	1.1	-0.1	0.7	-0.7	1.0	0.8	0.6
Mace Head	0.4	0.5	0.2	0.6	0.3	1.0	0.4	0.2
Melpitz	1.2	0.5	-0.7	0.8	-1.0	1.1	0.6	0.4
Montseny	2.6	3.1	0.5	1.8	0.0	0.7	0.4	0.1
Payerne	3.7	2.0	-1.7	2.1	-0.8	0.9	0.5	0.3
Puy de Dôme	0.6	0.9	0.3	0.8	0.2	0.9	0.2	0.1
Vavihill	2.8	1.1	-1.7	1.7	-1.2	1.2	0.8	0.7
VBS_BC_NEW	2.1	1.4	-0.6	1.2	-0.6	0.9	0.7	0.5
VBS_BC (Ciarelli et al., 2016a)	2.1	0.5	-1.5	1.6	-1.1	1.3	0.7	0.6

699

700

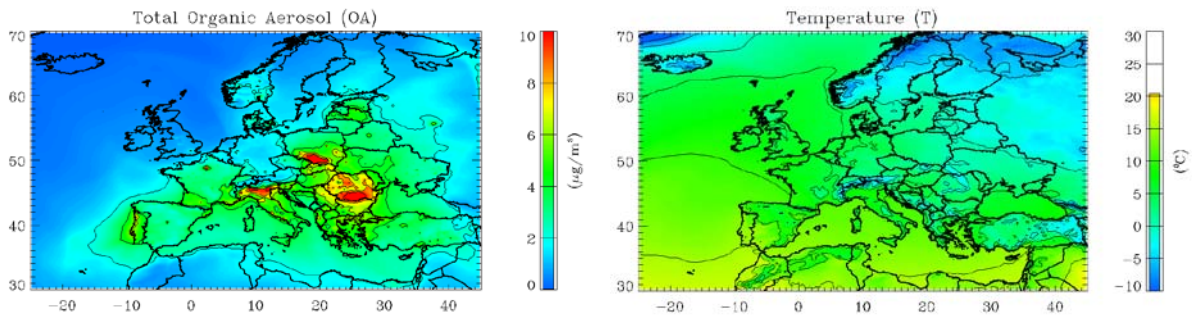
701

702

703

704

705

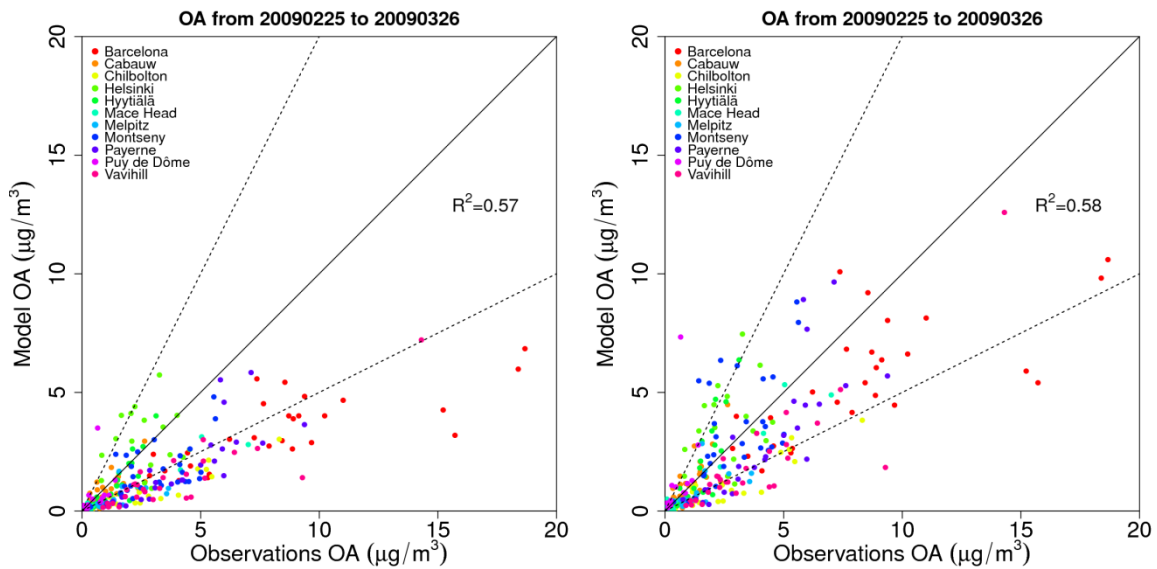


706

707 Figure 1. Modelled average total organic aerosol (OA) concentrations (VBC_BC_NEW) and
 708 surface temperature (T) for the period between 25 February and 26 March 2009.

709

710

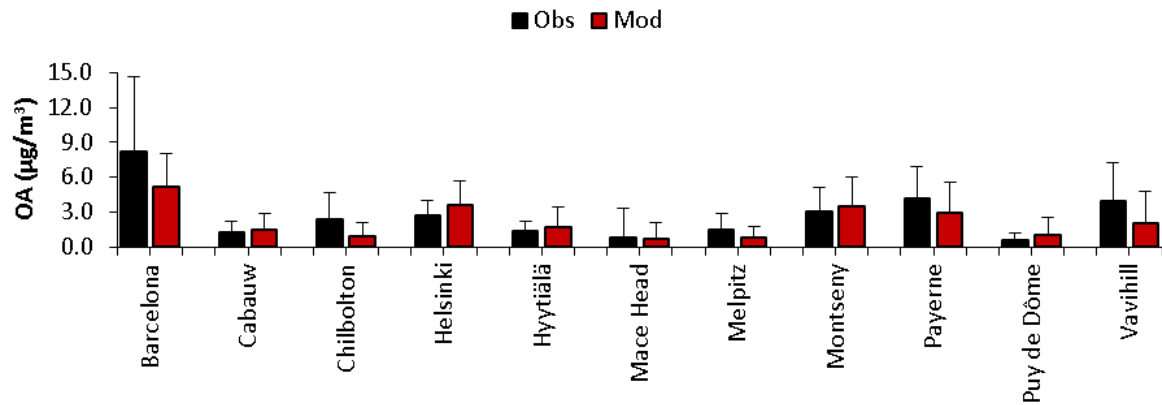


711

712 Figure 2. Daily average scatter plots for OA concentrations at 11 AMS sites for the period
 713 between 25 February and 26 March 2009 for VBS_BC (left) and VBS_BC_NEW case (right).
 714 Solid lines indicate the 1:1 line. Dotted lines are the 1:2 and 2:1 lines.

715

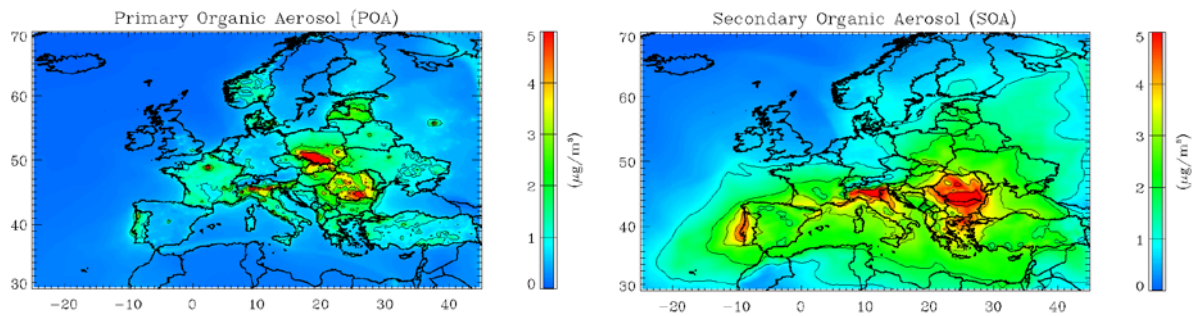
716



717

718 Figure 3. Observed (black) and modelled (VBS_BC_NEW) (red) average OA mass at AMS
719 sites for the period between 25 February and 26 March 2009.

720



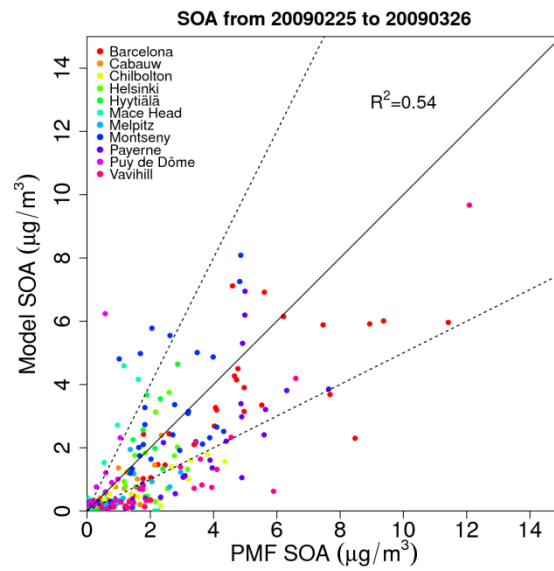
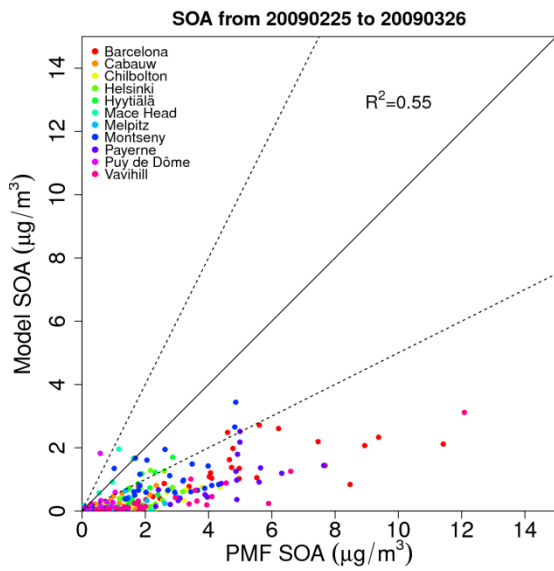
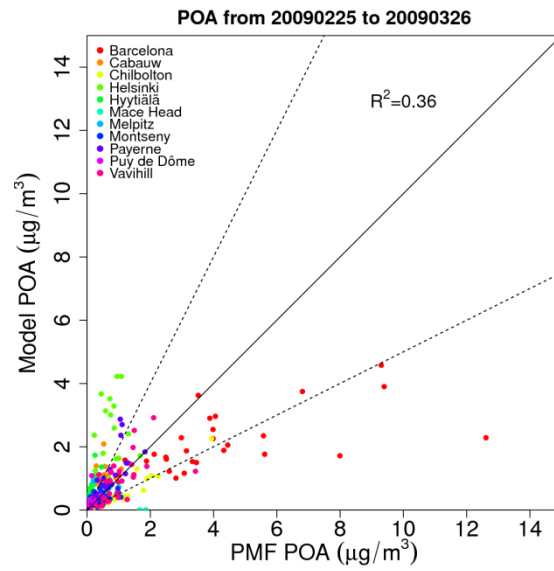
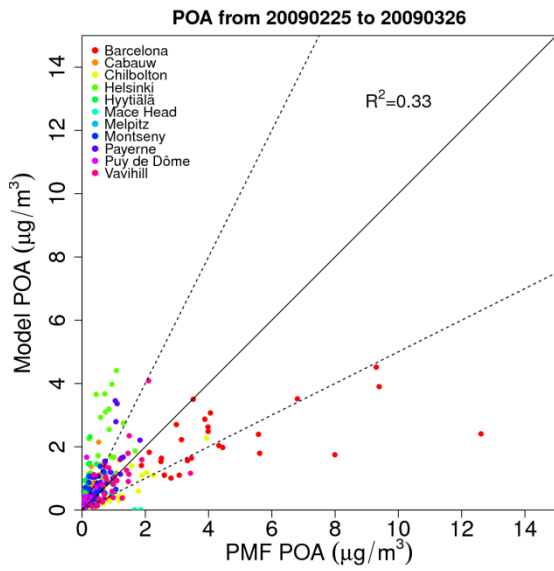
721

722 Figure 4. Modelled average POA (left) and SOA (right) concentrations for the period between
723 25 February and 26 March 2009.

724

725

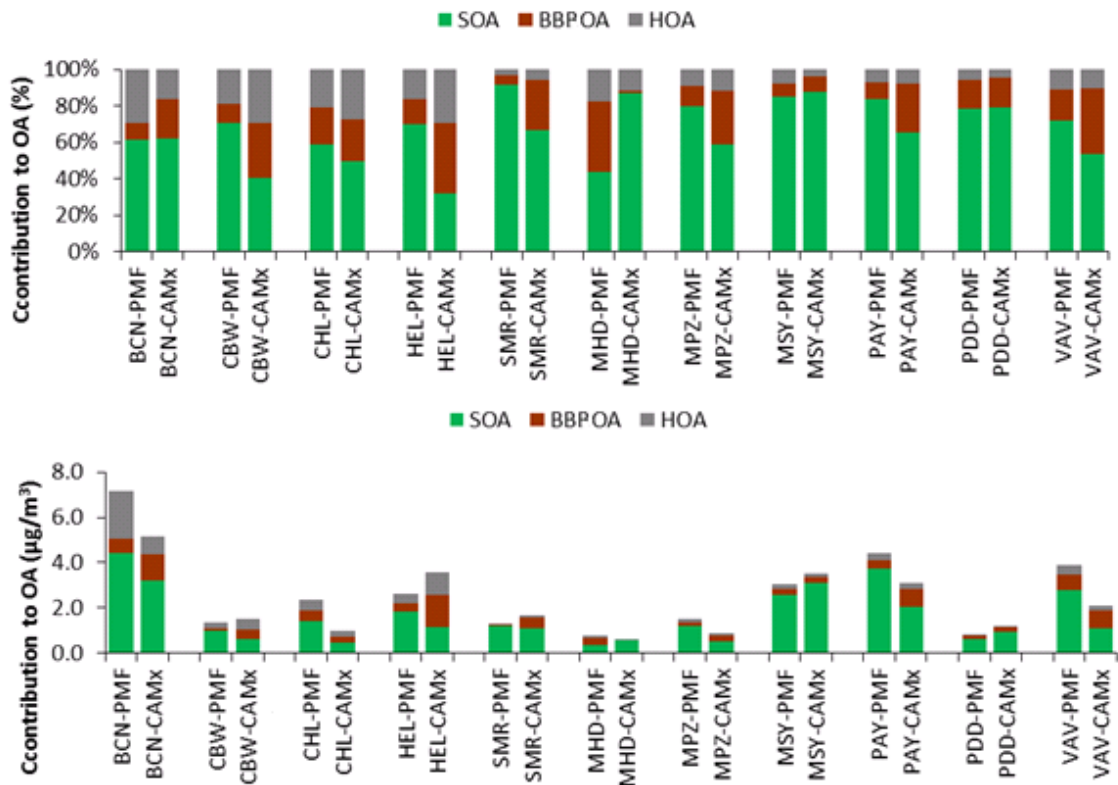
726



727

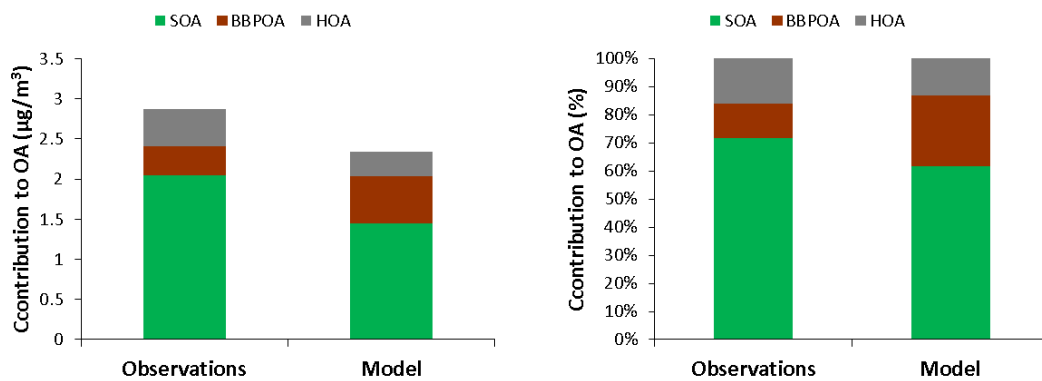
728

729 Figure 5. Daily average scatter plots of POA and SOA concentrations at 11 AMS sites for
 730 February-March 2009 in VBS_BC (Ciarelli et al., 2016a) (left) and VBS_BC_NEW (right).
 731 Solid lines indicate the 1:1 line. Dotted lines are the 1:2 and 2:1 lines.



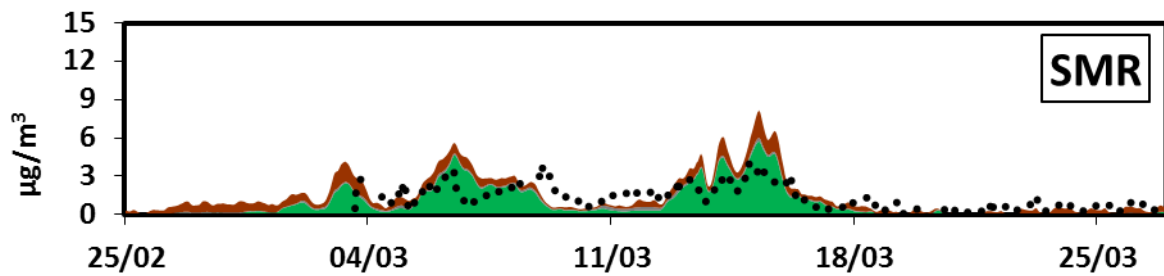
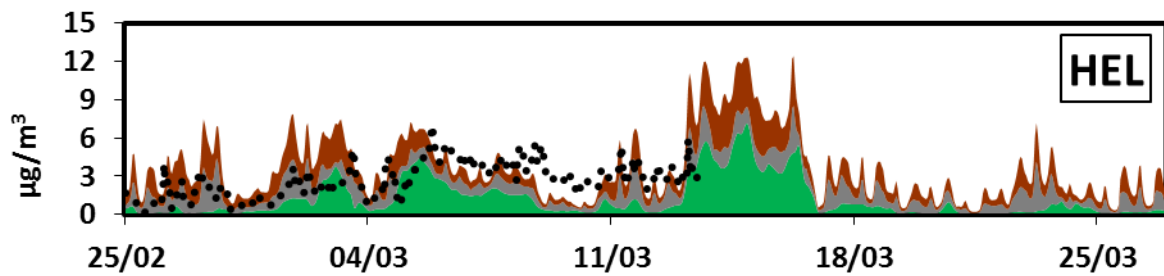
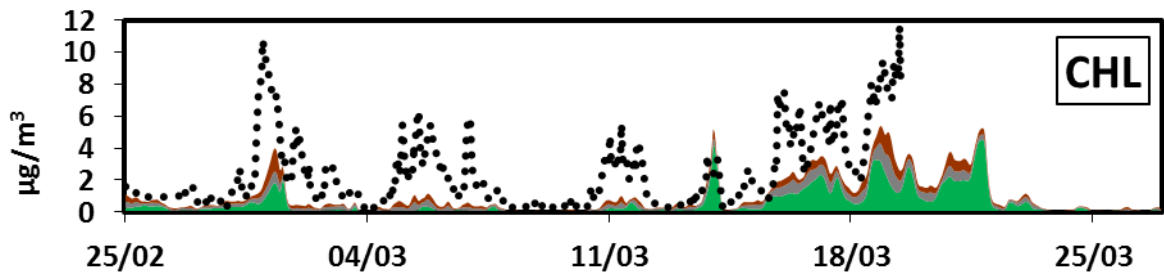
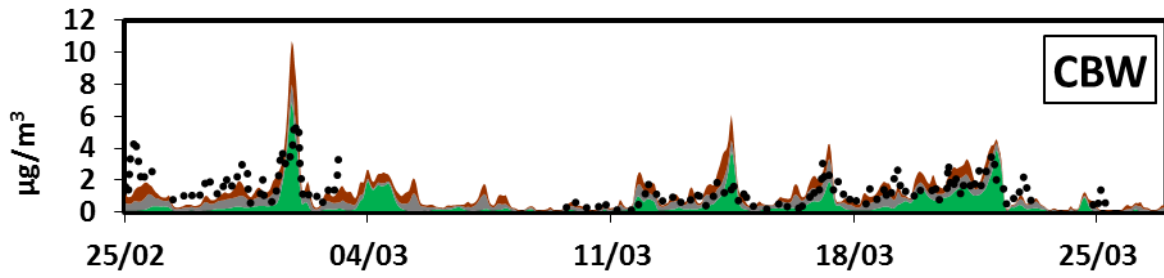
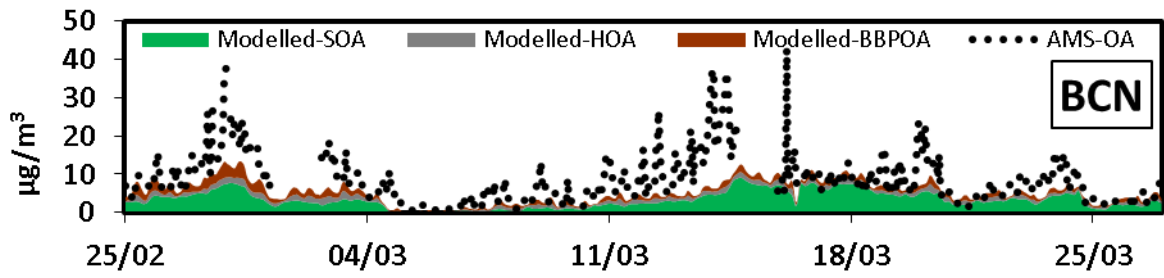
732

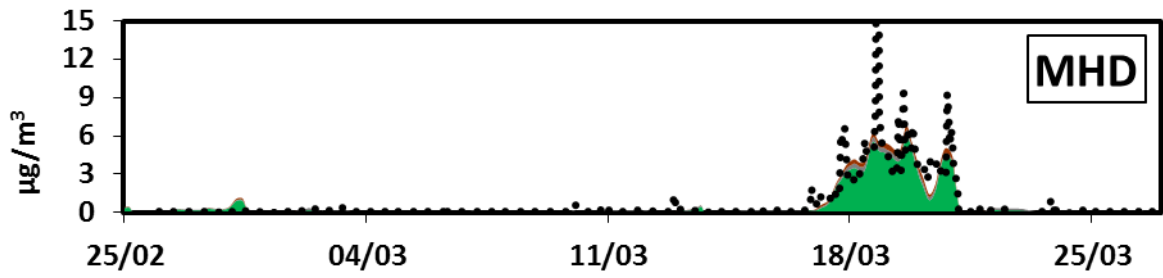
733 Figure 6. Relative (upper panel) and absolute (lower panel) contribution of HOA, BBPOA and
 734 SOA to OA concentrations at 11 sites from PMF analysis of AMS measurements (first bar)
 735 and CAMx VBS_BC_NEW results (second bar) for the period between 25 February and 26
 736 March 2009.



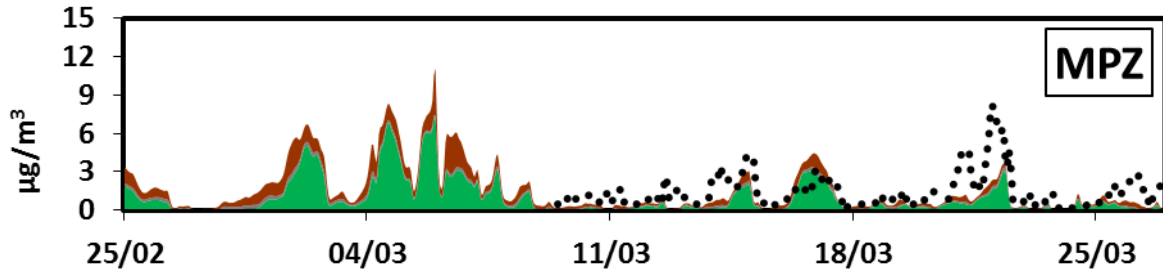
737

738 Figure 7. Measured and modelled average absolute (left panel) and relative (right panel)
 739 contributions of HOA, BBPOA and SOA to OA concentrations for all the 11 sites for the
 740 period between 25 February and 26 March 2009.

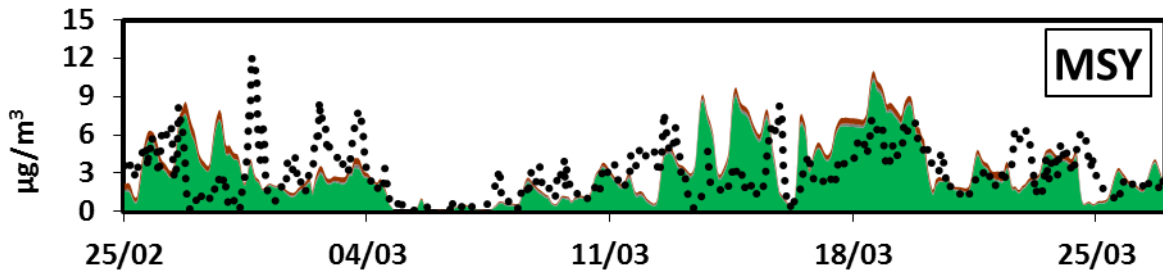




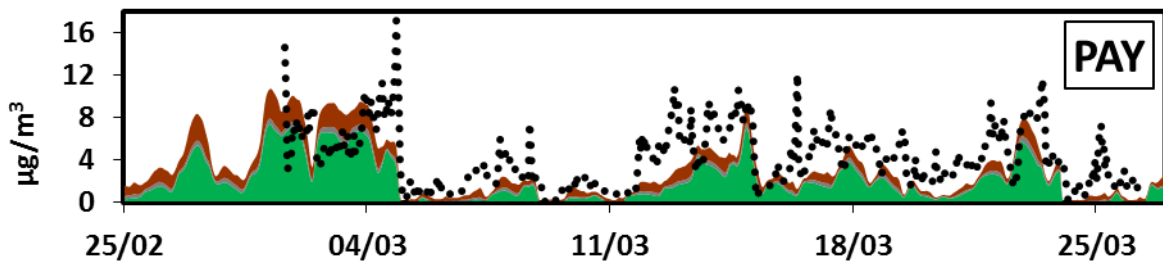
746



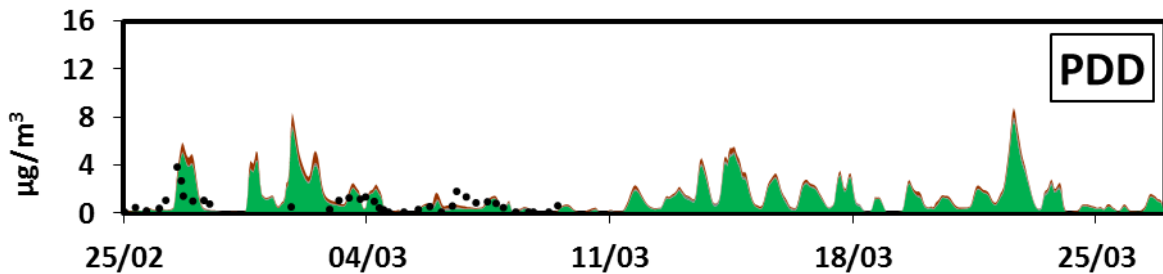
747



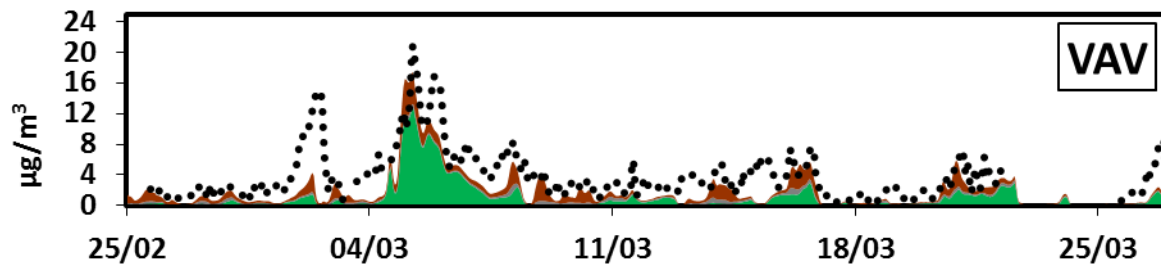
748



749

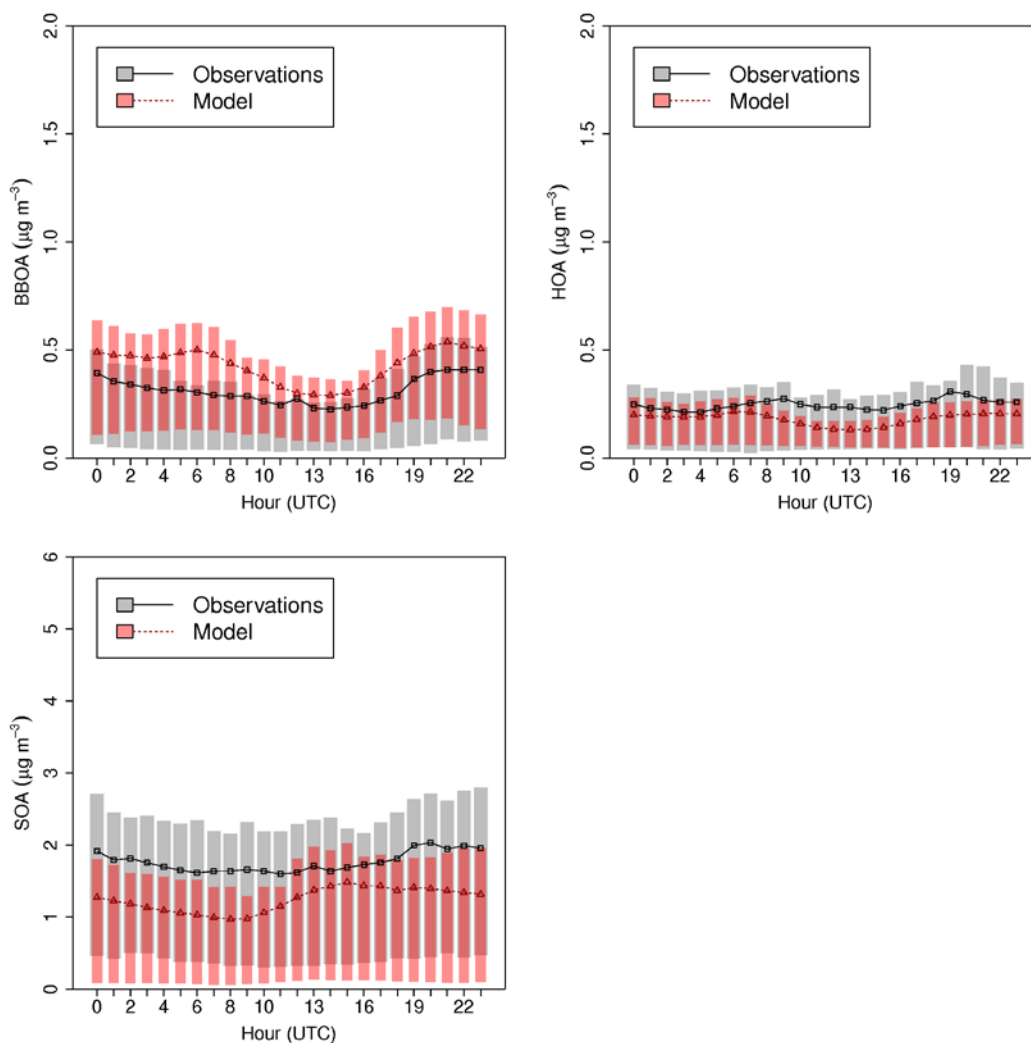


750

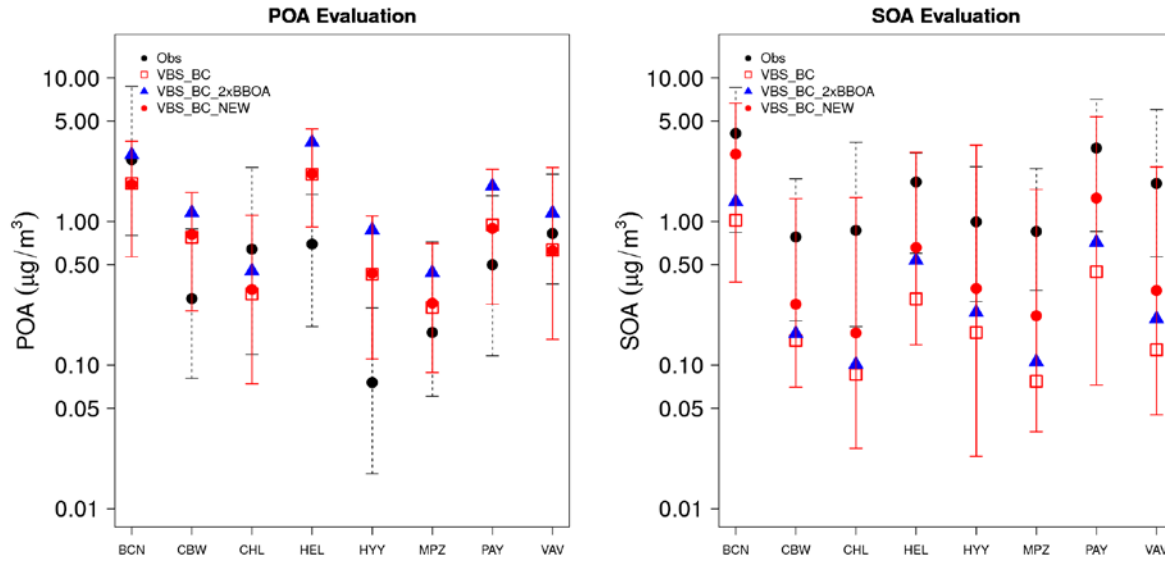


751
 752 Figure 8. Comparison of measured hourly OA mass concentrations (AMS-OA dotted line),
 753 with modelled components HOA, BBPOA and SOA.

754



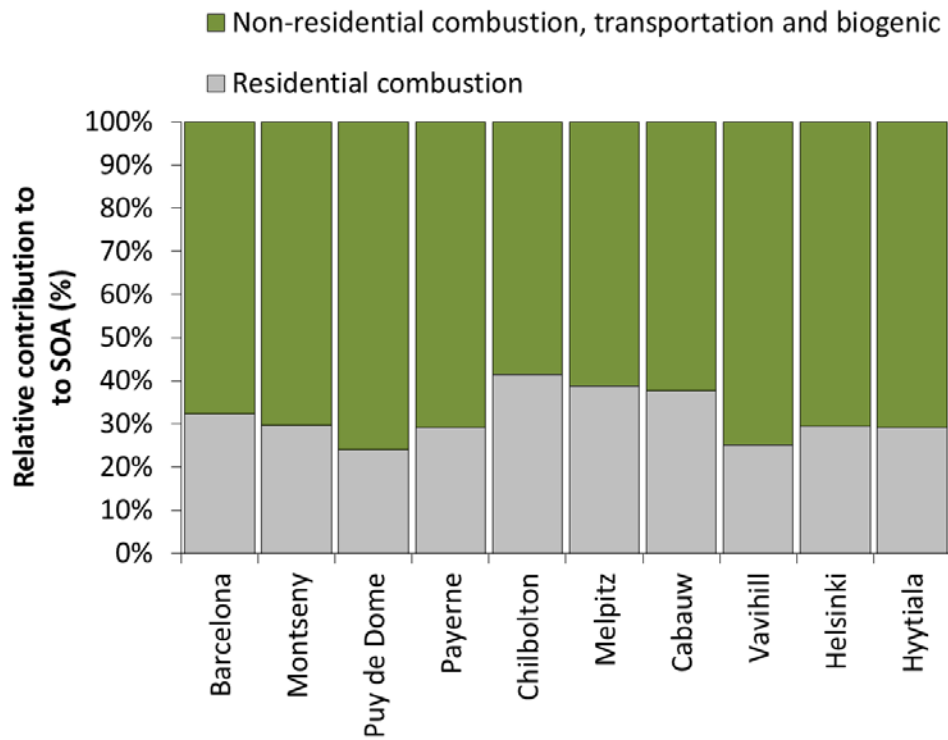
755
 756
 757 Figure 9. Comparison of modelled (red) and measured (grey) BBPOA, HOA and SOA diurnal
 758 profiles at the rural-background sites. The extent of the bars indicates the 25th and 75th
 759 percentiles.



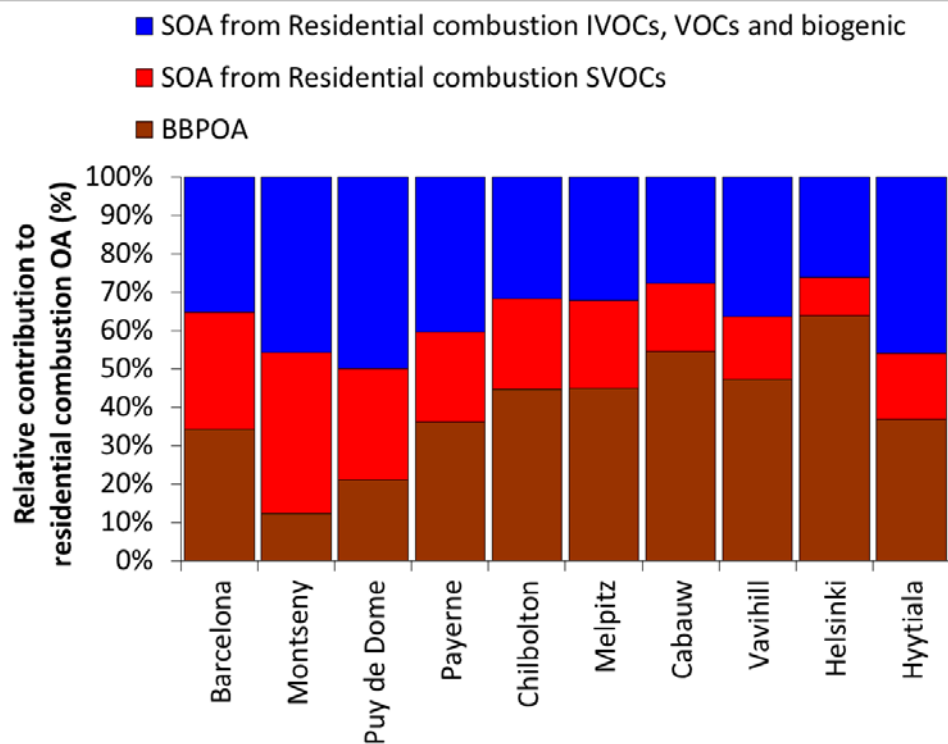
761
 762 Figure 10. POA (left) and SOA (right) median concentrations at 8 AMS sites for February-
 763 March 2009 in the VBS_BC, VBS_BC_2xBBOA and VBS_BC_NEW cases. Dotted lines
 764 indicate the 10th and 90th quartile range (also reported in red for the VBS_BC_NEW case).
 765 Data for the Puy de Dôme and Montseny sites at higher layers are not available for the
 766 VBS_BC_2xBBOA scenario.

767

768

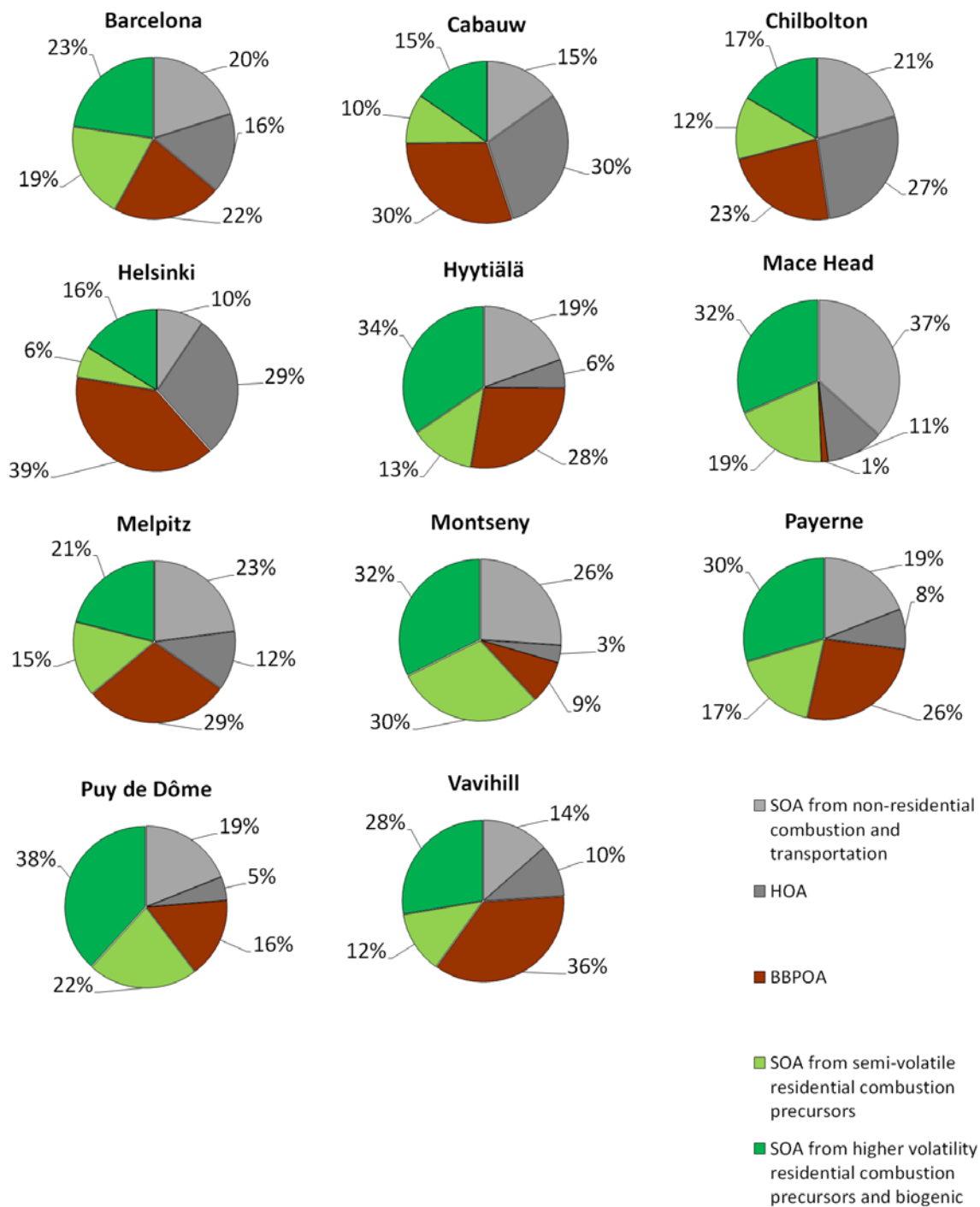


770



771

772 Figure 11. Contribution of residential and non-residential combustion precursors to SOA at
 773 different sites (upper panel). Contribution of BBPOA, SVOCs and higher volatility organic
 774 precursors to residential heating OA (lower panel). Stations are ordered from south to north.



776

777 Figure 12. Average modelled composition of OA at the 11 AMS sites for the period between
 778 25 February and 26 March 2009.

1 **5 Supplement**

2 Table S1. Statistics for model evaluation. M_i represents the modelled value, O_i the
 3 observations, \bar{O} the mean of the observations and n the total number of data points.

Mean Bias (MB)	$MB = \frac{1}{n} \sum_{i=1}^n (M_i - O_i),$
Mean Error (ME)	$ME = \frac{1}{n} \sum_{i=1}^n (M_i - O_i),$
Mean Fractional Bias (ME)	$MFB = \frac{2}{n} \sum_{i=1}^n \left(\frac{M_i - O_i}{M_i + O_i} \right),$
Mean Fractional Bias (ME)	$MFE = \frac{2}{n} \sum_{i=1}^n \left(\frac{ M_i - O_i }{M_i + O_i} \right),$
Coefficient of determination (R^2)	$R^2 = 1 - \frac{\sum_{i=1}^n (O_i - M_i)^2}{\sum_{i=1}^n (O_i - \bar{O})^2}.$

4
 5
 6
 7
 8
 9
 10
 11
 12
 13
 14
 15

1 Table S2. Statistical analysis for HOA during February-March 2009 periods at 11 AMS sites.

Site	Mean observed HOA ($\mu\text{g m}^{-3}$)	Mean modelled HOA ($\mu\text{g m}^{-3}$)	MB ($\mu\text{g m}^{-3}$)	ME ($\mu\text{g m}^{-3}$)	MFB [-]	MFE [-]	r	R ²
Barcelona	2.1	0.8	-1.3	1.5	-0.4	0.8	0.4	0.1
Cabauw	0.3	0.4	0.2	0.2	0.6	0.8	0.5	0.2
Chilbolton	0.5	0.3	-0.2	0.3	-0.5	0.7	0.8	0.6
Helsinki	0.4	1.0	0.6	0.7	0.8	0.9	0.2	0.1
Hyytiälä	0.0	0.1	0.1	0.1	0.7	0.8	0.6	0.3
Mace Head	0.1	0.1	-0.1	0.1	0.5	1.1	0.6	0.3
Melpitz	0.1	0.1	0.0	0.1	-0.1	0.6	0.6	0.3
Montseny	0.2	0.1	-0.1	0.2	-0.3	0.8	0.4	0.1
Payerne	0.3	0.3	-0.1	0.2	0.0	0.6	0.4	0.1
Puy de Dôme	0.0	0.1	0.0	0.0	0.3	0.8	0.1	0.0
Vavihill	0.4	0.2	-0.2	0.2	-0.4	0.7	0.5	0.2

2
3
4
5
6
7
8
9
10
11
12
13

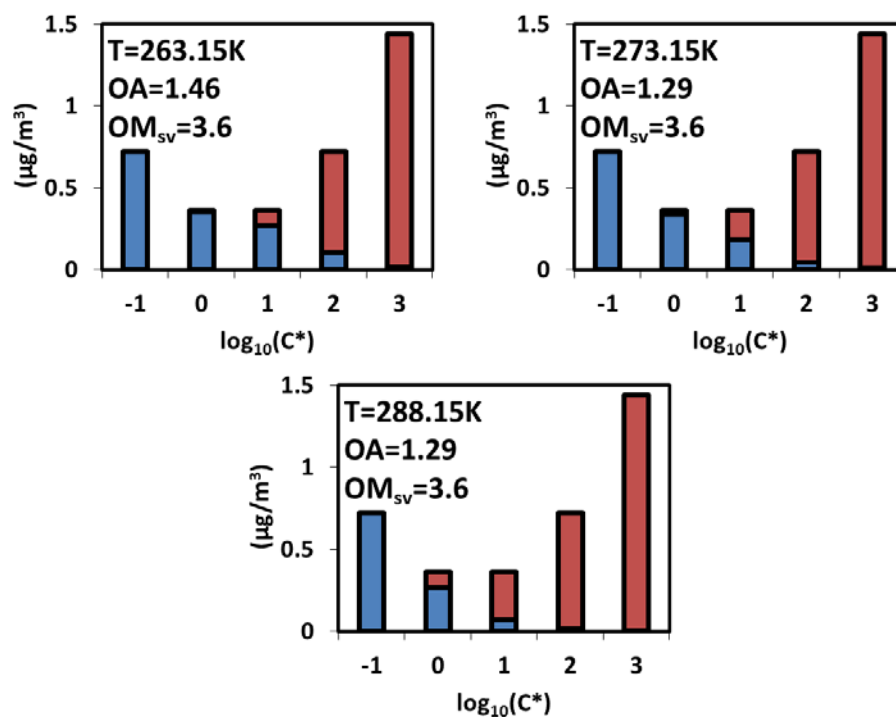
1 Table S3 Statistical analysis for BBPOA during February-March 2009 periods at 11 AMS
 2 sites.

Site	Mean observed BBPOA ($\mu\text{g m}^{-3}$)	Mean modelled BBPOA ($\mu\text{g m}^{-3}$)	MB ($\mu\text{g m}^{-3}$)	ME ($\mu\text{g m}^{-3}$)	MFB [-]	MFE [-]	r	R ²
Barcelona	0.7	1.1	0.5	0.7	0.6	0.8	0.4	0.2
Cabauw	0.1	0.5	0.3	0.3	1.0	1.1	0.5	0.3
Chilbolton	0.5	0.2	-0.3	0.3	-0.6	0.8	0.6	0.4
Helsinki	0.4	1.4	1.0	1.1	1.1	1.1	0.1	0.0
Hyytiälä	0.1	0.5	0.4	0.4	1.5	1.5	0.7	0.5
Mace Head	0.3	0.0	-0.3	0.3	-0.9	1.4	-0.1	0.0
Melpitz	0.2	0.3	0.1	0.2	0.7	0.9	0.4	0.2
Montseny	0.2	0.3	0.1	0.2	0.5	0.8	0.2	0.1
Payerne	0.4	0.8	0.4	0.5	0.8	0.9	0.6	0.3
Puy de Dôme	0.1	0.2	0.1	0.2	0.5	1.0	0.3	0.1
Vavihill	0.7	0.7	0.1	0.5	-0.1	0.7	0.5	0.2

3
 4 Table S4. Comparison of statistics for BBPOA in VBS_BC_NEW with VBS_BC (average of all sites
 5 in February-March 2009)
 6

	Mean obs ($\mu\text{g m}^{-3}$)	Mean mod ($\mu\text{g m}^{-3}$)	MB ($\mu\text{g m}^{-3}$)	ME ($\mu\text{g m}^{-3}$)	MFB [-]	MFE [-]
VBS_BC	0.36	0.60	0.24	0.45	0.47	0.98
VBS_BC_NEW	0.36	0.59	0.23	0.43	0.50	0.97

7



1

2

3 Figure S1. Box-model partitioning of biomass burning POA at about $1 \mu\text{g}/\text{m}^3$ OA at different
 4 temperatures (263.15, 273.15 and 288.15 K) using volatility distributions proposed by May et
 5 al. (2013). Particle phase is represented blue and gas phase in red. The lowest bin ($\log_{10}C^*=-1$)
 6 is used as a proxy for all non-volatile species which will only reside in the particle phase.

7

8

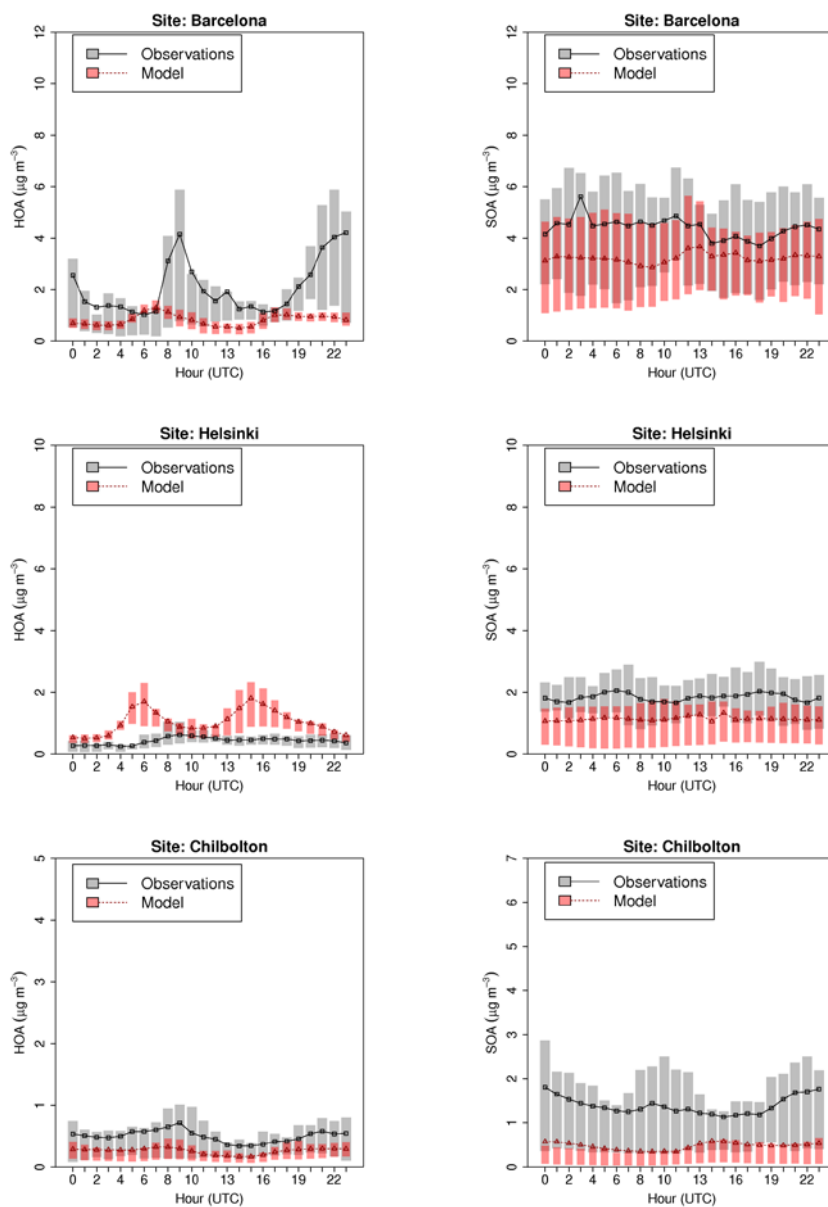
9

10

11

12

13



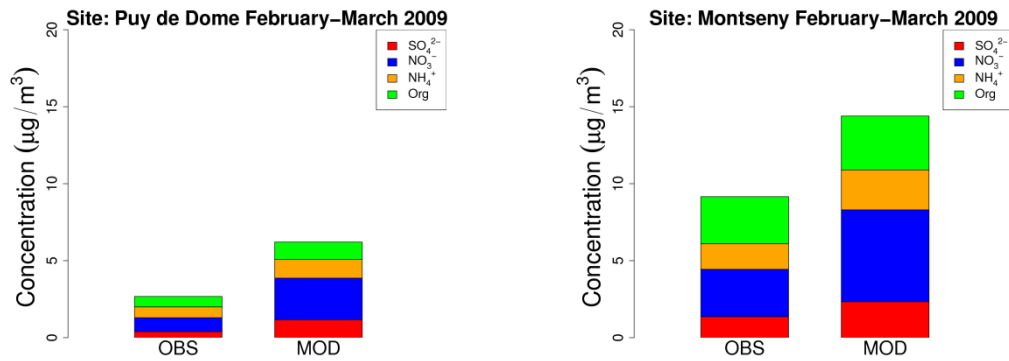
1

2

3

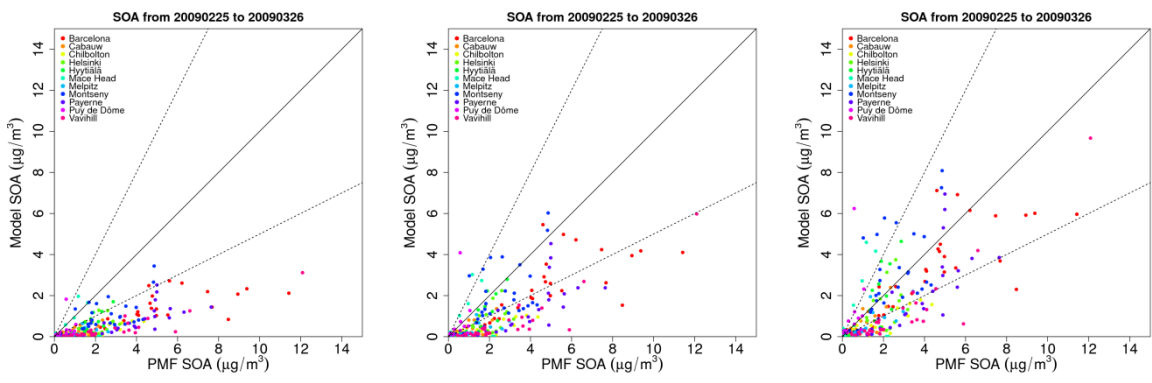
4 Figure S2. Comparison of modelled (red) and measured (grey) HOA and SOA diurnal profiles
 5 at the sites of Barcelona, Helsinki and Chilbolton. The extent of the bars indicates the 25th
 6 and 75th percentiles.

7



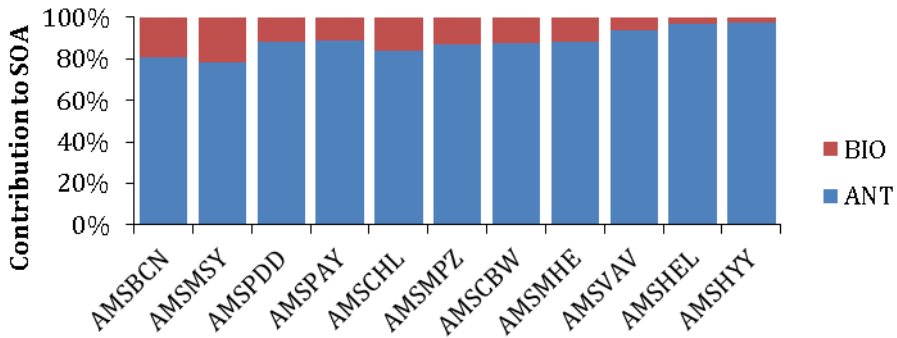
1
2 Figure S3. Comparison of modelled non-refractory PM25 components at Puy de Dome and
3 Montseny with the AMS measurements in February-March 2009.

4
5



6
7 Figure S4. Modelled versus PMF SOA; with VBS_BC (Ciarelli et al., 2016a) (left panel),
8 with VBS_BC where BBPOA vapours were allowed to be further oxidized (Koo et al. 2014)
9 (middle panel), and with VBS_BC_NEW (right panel).

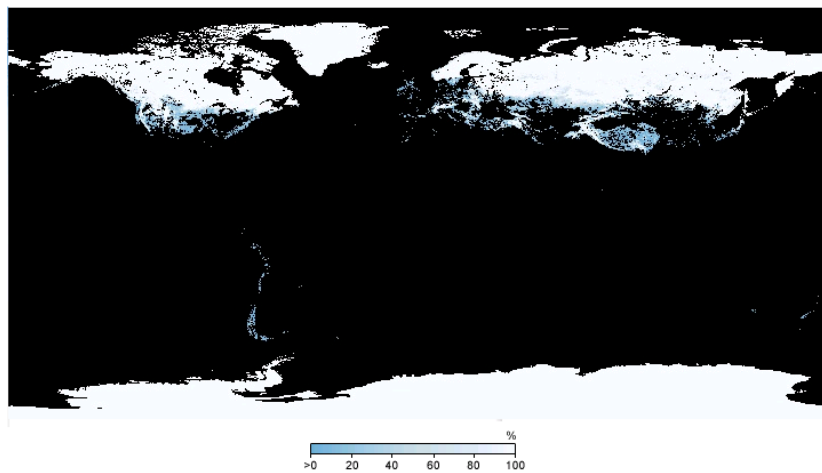
10



11
12 Figure S5. Biogenic and anthropogenic contribution to SOA at stations from south to north
13 retrieved as a difference between the predicted SOA in the reference simulation (including
14 biogenic) and a sensitivity test with no biogenic SOA formation.

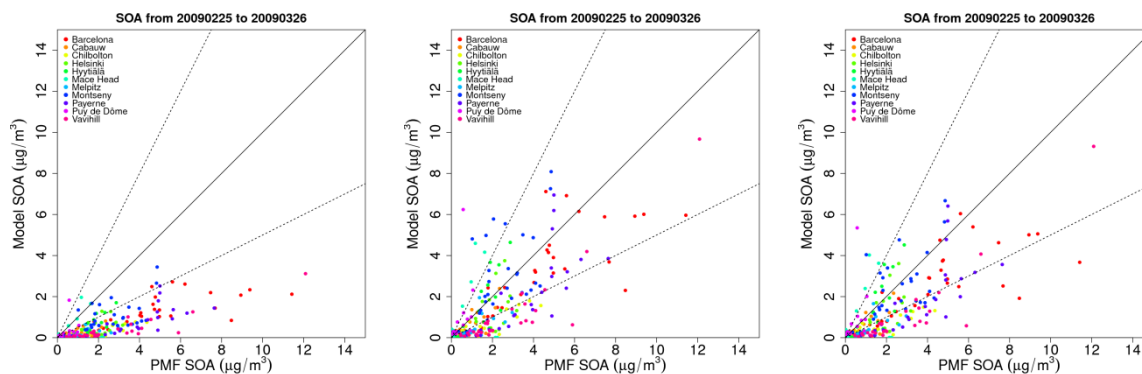
15
16
17
18
19

1



2
3
4
5

Figure S6. Snow cover for March 2009 as retrieved by the TERRA/MODIS instrument.



6
7
8
9
10
11
12
13
14
15

Figure S7. Modelled versus PMF SOA; with VBS_BC (Ciarelli et al., 2016a) (left panel), with VBS_BC_NEW (middle panel), and with VBS_BC_NEW but without biogenic SOA (right panel).